

Parton Momentum and Helicity Distributions in the Nucleon

P. Jimenez-Delgado¹, W. Melnitchouk¹, J. F. Owens²

¹ Jefferson Lab, Newport News, Virginia 23606, USA

² Department of Physics, Florida State University, Tallahassee, Florida 32306, USA

E-mail: wmelnitc@jlab.org

Abstract. We review the current status of spin-averaged and spin-dependent parton distribution functions (PDFs) of the nucleon. After presenting the formalism used to fit PDFs in modern global data analyses, we discuss constraints placed on the PDFs by specific data types. We give representative examples of unpolarized and polarized PDFs and their errors, and list open questions in global QCD fitting. Finally, we anticipate how future facilities, with fixed-target and collider experiments, may impact our knowledge of PDFs and reduce their uncertainties.

Contents

| | | |
|----------|---|-----------|
| 1 | Introduction | 3 |
| 2 | QCD Analysis | 4 |
| 2.1 | Running coupling | 5 |
| 2.2 | Q^2 evolution | 6 |
| 2.3 | Hard scattering processes | 7 |
| 2.3.1 | Lepton–hadron deep-inelastic scattering. | 7 |
| 2.3.2 | Hadron–hadron scattering. | 8 |
| 2.4 | Heavy quarks | 11 |
| 2.5 | Power corrections | 13 |
| 2.6 | Nuclear corrections | 15 |
| 2.7 | PDF parametrizations and sum rule constraints | 18 |
| 2.8 | PDF errors | 19 |
| 2.8.1 | Hessian method. | 20 |
| 2.8.2 | Lagrange multiplier method. | 20 |
| 2.8.3 | Monte Carlo method. | 21 |
| 2.9 | Data types | 21 |
| 2.9.1 | Unpolarized experiments. | 21 |
| 2.9.2 | Polarized experiments. | 23 |
| 3 | Unpolarized parton distributions | 25 |
| 3.1 | Valence quarks at large x | 27 |
| 3.2 | Light quark sea | 31 |
| 3.3 | Charge symmetry violation in PDFs | 33 |
| 3.4 | Strange quarks | 35 |
| 3.5 | Heavy quarks | 37 |
| 3.6 | Gluons | 39 |
| 3.7 | Lattice PDF moments | 43 |
| 4 | Spin-dependent parton distributions | 44 |
| 4.1 | Polarized valence quarks at large x | 46 |
| 4.2 | Polarized sea quarks | 49 |
| 4.3 | Gluon helicity | 51 |
| 5 | Outlook | 52 |

1. Introduction

Quantum Chromodynamics, the theory describing the interactions of quarks and gluons, has been shown to provide excellent descriptions of a wide variety of phenomena ranging from hadron spectroscopy via lattice field theory to hard scattering phenomena via perturbation theory. Yet QCD is a theory whose degrees of freedom are the quarks and gluons – quanta that can not be observed directly due to their confinement in hadrons. On the other hand, experiments deal with hadrons and leptons. In order to calculate observables measured in high energy scattering processes a technique is needed that allows conversion from a description in terms of hadrons to one in terms of quarks and gluons (collectively referred to as partons). For hadrons in the initial state this conversion is provided by parton distribution functions (PDFs), while for final state hadrons a similar role is played by parton fragmentation functions. The PDFs, denoted by $f_i(x)$, for each type of quark and antiquark and for the gluon ($i = q, \bar{q}, g$), allow one to essentially describe a beam of hadrons as an effective beam of quarks and gluons. In the infinite momentum frame, the PDFs can be interpreted as probability densities describing how the parent hadron’s momentum is shared amongst the different types of partons, as a function of the hadron’s momentum fraction x . With knowledge of the PDFs and the Feynman rules for QCD, one can calculate hard scattering cross sections and differential distributions that can then be compared to data.

PDFs are traditionally determined by simultaneously fitting a wide variety of data for large momentum transfer processes. The parameters of the fits describe the PDFs at some initial momentum transfer scale, while evolution equations are then used to calculate the PDFs at all other scales needed for the calculations. The data sets used for such fits often include deep inelastic scattering (DIS) of charged leptons on proton and deuterium targets, or neutrinos on heavy nuclear targets, lepton pair production on proton and deuterium targets, and the production of photons, vector bosons, or jets at large values of transverse momentum.

While the PDFs provide us with a detailed description of the partonic substructure of hadrons, they contain only partial information. Partons (both quarks and gluons) have nonzero spin, so that the fundamental distributions in nature are the PDFs for a specific helicity (spin projection along the direction of motion), f_i^\uparrow and f_i^\downarrow , corresponding to parton spins aligned and antialigned with that of the hadron, respectively. Experiments with unpolarized beams and targets are therefore sensitive only to the sums of the helicity PDFs, $f_i = f_i^\uparrow + f_i^\downarrow$, while information on the differences, $\Delta f_i = f_i^\uparrow - f_i^\downarrow$, can be obtained from measurements involving polarized beams and/or targets.

It is the purpose of this topical review to give a current “snapshot” of the status of our knowledge of PDFs, both unpolarized and polarized. To this end, brief reviews of both the theory and the types of data used in the fits will be presented, and theoretical issues that need to be addressed in the perturbative calculations will be outlined. Throughout this review we shall attempt to answer the question “what do we know

and how do we know it?” Recently there have been several excellent reviews of PDFs [1, 2, 3], updating the early treatises of PDFs in Refs. [4, 5], which have focused on various aspects of unpolarized PDFs, such as the impact on the phenomenology of the Large Hadron Collider (LHC). The spin structure of the nucleon, including spin-dependent PDFs, was also reviewed in Refs. [6, 7, 8]. The present pedagogical review should be viewed as complementary to these efforts, emphasizing the different aspects of hadron structure that can be revealed through the study of unpolarized and polarized PDFs, at both small and large parton momentum fractions x .

There is an old saying in experimental particle physics that “today’s discovery is tomorrow’s calibration.” A similar effect occurs for theoretical calculations. What was once touted as a test of QCD, now often plays the role of providing a description of backgrounds for searches for new types of particles. Of course, one wants these calculations to be as accurate as possible and this, in turn, requires precise knowledge of the PDFs that enter into the calculation. The error estimates on PDFs will be discussed at some length for this reason. On the other hand, there are many aspects of hadron structure that are currently not understood well, or at all, either theoretically or experimentally, and clearly identifying and delineating the limits of our knowledge in the context of global PDF fits serves a valuable purpose.

The plan of the review is as follows. Sec. 2 contains an overview of the necessary QCD theory required to understand the results of global fits. Sec. 3 contains the review of unpolarized PDFs, while Sec. 4 summarizes the status of polarized PDFs. Finally, Sec. 5 provides some speculations as to how our knowledge of PDFs may be improved through anticipated results of ongoing and future experiments.

2. QCD Analysis

As noted in the introduction, PDFs are necessary ingredients for obtaining predictions for hard scattering hadron–hadron and lepton–hadron processes. The cross section for a typical hadron–hadron process involving collisions of hadrons A and B , with momenta p_A and p_B , respectively, producing a state C in addition to other hadrons (collectively denoted by X), can be written in the form

$$\begin{aligned} \sigma_{AB \rightarrow CX}(p_A, p_B) &= \sum_{a,b} \int dx_a dx_b f_{a/A}(x_a, \mu_f) f_{b/B}(x_b, \mu_f) \\ &\quad \times \sum_n \alpha_s^n(\mu_r) \hat{\sigma}_{ab \rightarrow CX}^{(n)}(x_a p_A, x_b p_B, Q/\mu_f, Q/\mu_r), \end{aligned} \quad (1)$$

where $\hat{\sigma}^{(n)}$ denotes an n -th order parton–parton “cross section” that produces the desired final state, and the functions $f_{a/A}$ and $f_{b/B}$ are the PDFs of flavor a in hadron A and flavor b in hadron B , respectively. The state C might denote a high- p_T jet, a lepton pair, a photon or weak vector boson, for example, and Q is a scale that characterizes the hard scattering. For high- p_T jet or photon production the scale $Q \sim p_T$. The form (1) can also be applied to the case when the hadrons A and B are polarized; in the remainder of this section, however, we shall for illustration focus primarily on the unpolarized case.

The parton-level cross sections will generally possess ultraviolet singularities that must be renormalized. Doing so leads to the introduction of the running coupling $\alpha_s(\mu_r)$ which depends on a renormalization scale μ_r . There can also be infrared singularities associated with loop graphs; these will cancel corresponding singularities from the emission of real soft gluons, provided that the observable is suitably defined, *i.e.*, that it is “infrared safe.” Finally, there will be collinear singularities associated with, in this case, the initial partons emitting additional partons at zero angle. These collinear configurations correspond to internal propagators going on-shell and, as such, correspond to long-distance physics. Such singular terms can be *factorized* and absorbed into the PDFs. This process introduces a factorization scale, μ_f , that separates the long-distance and short-distance hard scattering physics.

As shown in Eq. (1), the partonic hard scattering cross section can be expanded in powers of the running coupling. The dependence on μ_r that enters via the running coupling cancels that which appears in the partonic cross sections. Similarly, the dependence on μ_f in the PDFs cancels against the μ_f dependence in the partonic cross sections. These cancellations represent the fact that the physical cross section, if calculated to all orders in perturbation theory, should not depend on the two scales introduced to control the ultraviolet and collinear singularities. However, at any fixed order in perturbation theory these cancellations will only be approximate. Indeed, at order α_s^m one has the relations

$$\mu_f^2 \frac{\partial \sigma_{AB \rightarrow CX}}{\partial \mu_f^2} = 0 + \mathcal{O}(\alpha_s^{m+1}), \quad \mu_r^2 \frac{\partial \sigma_{AB \rightarrow CX}}{\partial \mu_r^2} = 0 + \mathcal{O}(\alpha_s^{m+1}). \quad (2)$$

These results suggest that the dependence on the renormalization and factorization scale choices will decrease as one carries out the perturbative calculations to higher order. This is indeed the case for the processes typically used in global fits for PDFs. (If a new kinematic configuration opens up at a higher order, then the corrections at that order can be large. This happens when going from LO to NLO for heavy quark production, for example, in which case the scale dependence can actually increase at that order. The reduction then occurs at the next order.) These processes are all known to at least NLO and some to NNLO, as will be discussed below. In principle, the two scales μ_r and μ_f can be chosen independently. However, in processes where there is one large scale characterizing the hard scattering it is often the case that the choice $\mu_f = \mu_r \equiv \mu$ is used. This simplifying choice will be utilized in the results discussed in the sections to follow.

2.1. Running coupling

The dependence on the renormalization scale of the running coupling is governed by the QCD β function via the renormalization group equation,

$$\mu_r^2 \frac{\partial \alpha_s(\mu_r^2)}{\partial \mu_r^2} = \beta(\alpha_s(\mu_r^2)). \quad (3)$$

The QCD β function is calculable in perturbation theory and can be written as

$$\beta(\alpha_s) = -b_0\alpha_s^2 - b_1\alpha_s^3 - b_2\alpha_s^4 + \mathcal{O}(\alpha_s^5), \quad (4)$$

where the coefficients for n_f flavors are

$$b_0 = \frac{33 - 2n_f}{12\pi}, \quad (5)$$

$$b_1 = \frac{153 - 19n_f}{24\pi^2}, \quad (6)$$

$$b_2 = \frac{77139 - 15099n_f + 325n_f^2}{3456\pi^3}. \quad (7)$$

The strong coupling α_s calculated using the expression for β in Eq. (4) with terms up to b_n is referred to as the $(n + 1)$ -loop running coupling. LO calculations retain only b_0 , while NLO calculations retain b_1 , and NNLO calculations retain also b_2 . Note that the β function is negative, resulting in a decrease of α_s with increasing scale, a phenomenon known as asymptotic freedom. This behavior is essential for the applicability of perturbation theory for hard scattering processes.

2.2. Q^2 evolution

In Eq. (1) both the PDFs and the partonic cross sections depend on the factorization scale μ_f . As seen in Eq. (2), this scale dependence cancels up to the order of perturbation theory used. This fact allows one to calculate the μ_f^2 dependence of the PDFs. Indeed, the singularities associated with collinear parton emission are universal and factorize from the hard scattering subprocesses. The factorization scale dependence of the parton distributions is then also universal, reflecting the independence of physical quantities on the scale μ_f . This leads to the Q^2 evolution, or renormalization group equations (RGE),

$$\mu_f^2 \frac{\partial f_i(x, \mu_f^2)}{\partial \mu_f^2} = \sum_j \int_x^1 \frac{dy}{y} P_{ij} \left(\frac{x}{y}, \mu_f^2 \right) f_j(y, \mu_f^2) = \sum_j P_{ij} \otimes f_j, \quad (8)$$

where the Bjorken x variable is (related to) the longitudinal momentum fraction of the partons. The evolution kernels P_{ij} or “splitting functions” stem from the collinear divergences absorbed in the distributions and represent the (collinear) resolution of a parton i in a parton j . They are calculated perturbatively as a series expansion in $\alpha_s(\mu_f^2)$,

$$P_{ij} \left(\frac{x}{y}, \mu_f^2 \right) = \sum_{m=0}^{\infty} \left(\frac{\alpha_s(\mu_f^2)}{2\pi} \right)^{m+1} P_{ij}^{(m)} \left(\frac{x}{y} \right). \quad (9)$$

At present these have been computed up to 3 loops ($m = 2$), which is the necessary accuracy for a NNLO analysis.

The evolution of spin-dependent PDFs Δf_i follows in a similar manner, with a corresponding set of spin-dependent splitting functions ΔP_{ij} . In this case the splitting functions have been computed to 2 loops, enabling analyses to be performed at NLO accuracy.

2.3. Hard scattering processes

2.3.1. *Lepton-hadron deep-inelastic scattering.* Traditionally, information on the PDFs of the nucleon has come from the process of deep-inelastic scattering (DIS) of leptons from protons or nuclei, beginning with the pioneering experiments at SLAC in the late 1960s. In the one-boson exchange approximation, the differential DIS cross section can be written as a product of lepton and hadron tensors,

$$\frac{d^2\sigma}{d\Omega dE'} = \frac{\alpha^2}{Q^4} \frac{E'}{E} \sum_j \eta_j L_{\mu\nu}^j W_j^{\mu\nu}, \quad (10)$$

where α is the fine structure constant, $\Omega = \Omega(\theta, \phi)$ is the laboratory solid angle of the scattered lepton, and $E(E')$ is the incoming (outgoing) lepton energy. For neutral-currents, the summation is over $j = \gamma, Z$ and the interference γZ , while for charged-currents only W^\pm exchange contributes. The leptonic tensor $L_{\mu\nu}$ depends on the charge $e = \pm 1$ and helicity $\lambda = \pm 1$ of the lepton,

$$\begin{aligned} L_{\mu\nu}^\gamma &= 2 (k_\mu k'_\nu + k'_\mu k_\nu - g_{\mu\nu} k \cdot k' - i\lambda \varepsilon_{\mu\nu\alpha\beta} k^\alpha k'^\beta), \\ L_{\mu\nu}^Z &= (g_V^e + e\lambda g_A^e) L_{\mu\nu}^{\gamma Z} = (g_V^e + e\lambda g_A^e)^2 L_{\mu\nu}^\gamma, \\ L_{\mu\nu}^W &= (1 + e\lambda)^2 L_{\mu\nu}^\gamma, \end{aligned} \quad (11)$$

where k and k' are the initial and final electron momenta, and $g_V^e = -1/2 + 2\sin^2\theta_W$ and $g_A^e = -1/2$ are the electron vector and axial-vector charges, respectively. The factors η_j in Eq. (10) denote the ratios of the corresponding propagators and couplings to the photon propagator and coupling squared [9]

$$\begin{aligned} \eta_\gamma &= 1, & \eta_Z &= \eta_{\gamma Z}^2 = \left(\frac{G_F M_Z^2}{2\sqrt{2}\pi\alpha} \right)^2 \frac{1}{(1 + M_Z^2/Q^2)^2}, \\ \eta_W &= \frac{1}{2} \left(\frac{G_F M_Z^2}{2\sqrt{2}\pi\alpha} \right)^2 \frac{1}{(1 + M_W^2/Q^2)^2}, \end{aligned} \quad (12)$$

where G_F is the Fermi weak interaction coupling constant, and M_W is the W boson mass.

The hadronic tensor $W_{\mu\nu}$ contains all of the information about the structure of the hadron target. Using constraints from Lorentz and gauge invariance, together with parity conservation, it can be decomposed into spin-independent and spin-dependent contributions,

$$\begin{aligned} W_{\mu\nu} &= -\tilde{g}_{\mu\nu} F_1(x, Q^2) + \frac{\tilde{p}_\mu \tilde{p}_\nu}{p \cdot q} F_2(x, Q^2) + i\varepsilon_{\mu\nu\alpha\beta} p^\alpha q^\beta F_3(x, Q^2) \\ &\quad + i\varepsilon_{\mu\nu\alpha\beta} \frac{q^\alpha}{p \cdot q} \left[s^\beta g_1(x, Q^2) + \left(s^\beta - \frac{s \cdot q}{p \cdot q} p^\beta \right) g_2(x, Q^2) \right], \end{aligned} \quad (13)$$

where p_μ and q_μ are the nucleon and exchanged boson four-momenta, $\tilde{g}_{\mu\nu} = g_{\mu\nu} - q_\mu q_\nu / q^2$, and $\tilde{p}_\mu = p_\mu - (p \cdot q / q^2) q_\mu$. The nucleon polarization four-vector s^β satisfies $s^2 = -1$ and $p \cdot s = 0$.

For spin-averaged scattering, the nucleon structure is parametrized in terms of the vector F_1 and F_2 structure functions, and the vector-axial vector interference F_3

structure function, which requires weak currents. These are generally functions of two variables (such as x and Q^2), but become functions of x only in the Bjorken limit, in which both Q^2 and $\nu \rightarrow \infty$, but x is fixed. In this limit the F_1 and F_2 structure functions become proportional, according to the Callan-Gross relation, $F_2(x) = 2xF_1(x)$, and in the parton model are given in terms of quark q and antiquark \bar{q} distribution functions,

$$F_1(x) = \frac{1}{2} \sum_q e_q^2 [f_q(x) + f_{\bar{q}}(x)], \quad (14)$$

where $f_q(x)$ is interpreted as the probability to find a quark of flavor q and charge e_q in the nucleon with light-cone momentum fraction x . At finite energies, the logarithmic Q^2 dependence from the evolution equations described in Sec. 2.2, as well as residual Q^2 dependence associated with power corrections (see Sec. 2.5 below), give corrections to the simple parton model expectations.

The spin-dependent structure functions g_1 and g_2 can be extracted from measurements where longitudinally polarized leptons are scattered from a target that is polarized either longitudinally or transversely relative to the electron beam. For longitudinal beam and target polarization, the difference between the cross sections for spins aligned and antialigned is dominated at high energy by the g_1 structure function. The g_2 structure function can be determined with additional measurement of cross sections for a nucleon polarized in a direction transverse to the beam polarization. In practice one often measures the polarization asymmetry A_1 , which is given as a ratio of spin-dependent and spin-averaged structure functions,

$$A_1(x, Q^2) = \frac{1}{F_1(x, Q^2)} \left[g_1(x, Q^2) - \frac{4M^2 x^2}{Q^2} g_2(x, Q^2) \right]. \quad (15)$$

At small values of x^2/Q^2 , one then has $A_1 \approx g_1/F_1$. If the Q^2 dependence of the polarized and unpolarized structure functions is similar, the polarization asymmetry A_1 will be weakly dependent on Q^2 .

In analogy with the unpolarized F_1 structure function, in the parton model the structure function g_1 can be expressed at LO in terms of differences between quark distributions with spins aligned (q_f^\uparrow) and antialigned (f_q^\downarrow) relative to that of the nucleon, $\Delta f_q(x) = f_q^\uparrow(x) - f_q^\downarrow(x)$,

$$g_1(x) = \frac{1}{2} \sum_q e_q^2 [\Delta f_q(x) + \Delta f_{\bar{q}}(x)]. \quad (16)$$

The g_2 structure function, on the other hand, does not have a simple parton model interpretation. However, its measurement provides important information on the subleading, higher twist contributions which parametrize long-range nonperturbative parton-parton correlations in the nucleon (see Sec. 2.5).

2.3.2. Hadron-hadron scattering. As discussed in Sec. 2, the PDFs are universal, the collinear singularities associated with initial parton collinear emission having been absorbed into the PDFs. Therefore, the parton distributions appearing, for example,

in the expressions for DIS structure functions, are the same that describe the structure of the incoming hadrons in hadronic production. Repeating the general form given in Eq. (1) (with $\mu_f = \mu_r \equiv \mu$), one has, for spin-unpolarized scattering,

$$\begin{aligned} \sigma_{AB \rightarrow CX}(p_A, p_B) &= \sum_{a,b} \int dx_a dx_b f_{a/A}(x_a, \mu) f_{b/B}(x_b, \mu) \\ &\times \sum_n \alpha_s^n(\mu) \hat{\sigma}_{ab \rightarrow CX}^{(n)}(x_a p_A, x_b p_B, Q/\mu), \end{aligned} \quad (17)$$

and an analogous expression for the spin-dependent cross section, involving the difference of cross sections with hadrons A and B polarized in the same and opposite directions,

$$\begin{aligned} \Delta\sigma_{\bar{A}\bar{B} \rightarrow CX}(p_A, p_B) &= \sum_{a,b} \int dx_a dx_b \Delta f_{a/A}(x_a, \mu) \Delta f_{b/B}(x_b, \mu) \\ &\times \sum_n \alpha_s^n(\mu) \Delta\hat{\sigma}_{\bar{a}\bar{b} \rightarrow CX}^{(n)}(x_a p_A, x_b p_B, Q/\mu). \end{aligned} \quad (18)$$

Here $\Delta f_{a/A}$ and $\Delta f_{b/B}$ are the spin-dependent PDFs for flavor a in a hadron A and flavor b in a hadron B , respectively, and $\Delta\hat{\sigma}^{(n)}$ is the corresponding spin-dependent partonic cross section. As indicated in Eqs. (17) and (18), the partonic cross sections are calculable in fixed-order perturbation theory as series expansions in $\alpha_s(\mu^2)$, which starts with different powers depending on the process.

It will be useful for subsequent sections to describe the parton kinematics for several examples of hadron-hadron processes. Although all processes used in global fits are known at least to NLO, the LO parton kinematics nevertheless serves as a useful guide to what region of parton momentum fraction and which combinations of parton flavors will be constrained by a given set of data.

Consider high- p_T dijet production in lowest order where two jets are produced with approximately balancing transverse momenta p_T and rapidities denoted by y_1 and y_2 . Two-body phase constrains the momentum fractions to be

$$x_a = \frac{x_T}{2} (e^{y_1} + e^{y_2}) \quad \text{and} \quad x_b = \frac{x_T}{2} (e^{-y_1} + e^{-y_2}), \quad (19)$$

where the dimensionless ratio $x_T = 2p_T/\sqrt{s}$. For centrally produced dijets one sees that the parton momentum fractions are both approximately x_T . However, if one or both of the jets is produced at far forward or backward rapidity values, then the x range can be considerably expanded towards large or small values thereby allowing a ‘‘tuning’’ of the probed x range.

For the case of inclusive production of a jet with transverse momentum p_T and rapidity y there is, at LO, an integration over one of the parton momentum fractions, say x_a , given by

$$\frac{x_T e^y}{2 - x_T e^{-y}} \leq x_a \leq 1 \quad \text{with} \quad x_b = \frac{x_a x_T e^{-y}}{2x_a - x_T e^y}. \quad (20)$$

Again, one sees that for y near 0 the ranges of the momentum fractions are centered near x_T .

Another important class of experiments involves the production of a system of mass M_B , rapidity y , and transverse momentum p_T . Examples of such systems include W^\pm , Z^0 , and charged lepton pairs l^+l^- . The four-momentum of the produced system is conveniently given as

$$(E; p_x, p_y, p_z) \equiv (m_T \cosh y; p_T \sin \phi, p_T \cos \phi, m_T \sinh y), \quad (21)$$

where $m_T^2 \equiv M_B^2 + p_T^2$, and ϕ is the azimuthal angle. The rapidity y and, equivalently, the Feynman- x variable x_F are defined by

$$y = \frac{1}{2} \ln \left(\frac{E + p_z}{E - p_z} \right), \quad x_F = \frac{p_z}{p_z^{\max}} \simeq \frac{2p_z}{\sqrt{s}}, \quad (22)$$

which lead to the relations [10, 11, 12]

$$x_F = 2\sqrt{(\tau + p_T^2/s)} \sinh y \iff y = \operatorname{arcsinh} \frac{x_F}{\sqrt{4\tau + x_T^2}}, \quad (23)$$

where $\tau \equiv M_B^2/s \simeq x_a x_b$.

Depending on the detected final state it is possible to define different cross sections for hadron-hadron collisions. In the Drell-Yan mechanism [13] a quark from one hadron and an antiquark from the other one annihilate into an intermediate vector boson (γ^* , Z^0 or W^\pm) which subsequently decays into a lepton pair. For lepton pairs of invariant mass $M_B \ll M_Z$, the process is dominated by virtual photon exchange. The experiments usually consist of proton (beam)-nucleon (proton or some other nucleus) collisions and the cross sections are extracted from the detection of muon pairs (dimuon production) produced in the decay of the virtual photons.

The double differential cross section for lepton pair production at LO is given by

$$\frac{d^2\sigma}{dM_B^2 dy} = \frac{4\pi\alpha^2}{9sM_B^2} \left[\sum_q e_q^2 f_q(x_a, \mu^2) f_{\bar{q}}(x_b, \mu^2) + (q \leftrightarrow \bar{q}) \right], \quad (24)$$

where the two parton momentum fractions are given by

$$x_a = \frac{M_B}{\sqrt{s}} e^y \quad \text{and} \quad x_b = \frac{M_B}{\sqrt{s}} e^{-y}. \quad (25)$$

From Eq. (24) one can see that for pp or pd collisions this process is sensitive separately to sea and valence distributions, in contrast to the neutral current DIS cross sections, where they enter as $q + \bar{q}$. Inclusion of the Drell-Yan data in global QCD analyses of PDFs is in fact instrumental in fixing ratio $\bar{d}/\bar{u} \approx \sigma^{pd}/\sigma^{pp} - 1$ for $x_a \gg x_b$ at LO (see Eq. (40) below). Another alternative is the use of charged current neutrino DIS structure functions, although this process entails the use of model dependent corrections for the heavy nuclear targets typically employed in such measurements. Nuclear corrections can be avoided if one instead uses the time reversed processes such as $e^\pm p \rightarrow \bar{\nu}_e(\nu_e) X$.

A process closely related to Drell-Yan dilepton production is the hadronic production of electroweak bosons [11, 12, 14]. For pp scattering, the inclusive production cross section for W^\pm bosons, for example, is given at LO by

$$\frac{d\sigma}{dy} = \frac{2\pi G_F}{3\sqrt{2}} \sum_{q, \bar{q}'} |V_{q\bar{q}'}|^2 x_a x_b f_q(x_a, M_W^2) f_{\bar{q}'}(x_b, M_W^2), \quad (26)$$

where $V_{q\bar{q}'}$ are the CKM matrix elements, and the sum runs over all light quark and antiquark flavors in both hadrons. The production of W^+ bosons is then sensitive primarily to the products $u(x_a)\bar{d}(x_b) + \bar{d}(x_a)u(x_b)$, while W^- production is sensitive to $d(x_a)\bar{u}(x_b) + \bar{u}(x_a)d(x_b)$. At large W boson rapidity, or equivalently $x_a \gg x_b$, W^\pm production is sensitive to the u and d quark PDFs in the proton, respectively. Provided the antiquark distributions at x_b are known to sufficiently accuracy, the W^-/W^+ cross section ratio would then be a clean probe of the d/u PDF ratio, which is presently not well determined at large x_a . Conversely, if the quark PDFs are known in particular regions of $x_{a,b}$, then the W^+/W^- ratios can also be used to probe the antiquark distributions.

Similar considerations apply when one or both of the protons are polarized, as for the case of the spin program at RHIC. For collisions of longitudinally polarized protons from unpolarized protons, $\vec{p}p \rightarrow W^\pm X$, the generalization of Eq. (26) simply involves replacing one of the quark or antiquark distributions by the corresponding polarized quark (antiquark) PDF, $\Delta f_{q(\bar{q})}$. Single-spin asymmetries can then constrain ratios of polarized to unpolarized PDFs, $\Delta f_{q(\bar{q})}/f_{q(\bar{q})}$, for various flavors, over specific regions of $x_{a,b}$ (see Sec. 4.2). Double-spin asymmetries, formed by combinations of inclusive hadron or jet production cross sections in the scattering of polarized protons from polarized protons, $\vec{p}\vec{p} \rightarrow (\text{hadron or jet}) X$, have also been studied in order to constrain the polarized gluon distribution Δg (see Sec. 4.3).

2.4. Heavy quarks

The treatment of heavy quarks in high-energy processes generally requires more care than for light quarks. The production mechanism of heavy quarks in DIS is predominantly the photon–gluon fusion (PGF) process, which makes it particularly sensitive to the gluon distribution in the nucleon. Although in principle there could exist an “intrinsic” (initial state) heavy quark content of the nucleon, existing measurements are well described through “extrinsic” (generated in the hard scattering) heavy quark production only (*cf.* [15] and references therein), so that any intrinsic heavy quark content of the nucleon is small and restricted to large values of Bjorken x (see Sec. 3.5 below).

The natural framework for describing the PGF mechanism is known as the “fixed flavor number scheme” (FFNS). In this approach the light-quark flavors (u, d, s) and the gluon are considered as massless partons within the nucleon. This scheme allows one to compute the contributions of heavy quarks (c, b, t) perturbatively as final-state quantum fluctuations, taking into account the full dependence of the production cross section on the mass m of the heavy quark. As is common in the $\overline{\text{MS}}$ renormalization scheme, the evaluation of the strong running coupling $\alpha_s(\mu^2)$ is nevertheless based on the usual variable flavor number scheme for the β -function governing its scale dependence. This procedure automatically resums the contributions to the strong coupling from heavy quarks, and consequently improves the stability of the perturbative expansion [16].

Complete calculations of (heavy-quark) DIS structure functions are presently known at LO [17, 18, 19, 20] and at NLO [21, 22]. Beyond this, approximations based on threshold resummation have been made [23, 24] (NNLO* in Sec. 3.5), but thus far the NNLO coefficient functions are only partially known [25, 26, 27], which constitutes a major drawback of any precision QCD analysis at NNLO accuracy. Another aspect of these calculations is the mass definition used; while the original calculations of the amplitudes employ the pole mass definition, it has been reported [28] that the use of the running mass definition improves the stability of the perturbative series.

In many situations calculations within the (fully massive) FFNS scheme become unduly complicated, and in many cases even impossible due to the unknown massive ($m \neq 0$) matrix elements at NNLO or even NLO. For this reason it is common to generate parton distributions in the so-called “variable flavor number scheme” (VFNS), where the heavy quarks are also considered to be massless constituents of the nucleon. Here, the required NLO and NNLO cross sections have been computed for a variety of important production processes, in particular at hadron colliders. In the VFNS scheme the effective heavy quark distributions are generated perturbatively from the nonperturbative distributions of light quarks and gluons using the boundary conditions of Ref. [29], typically at the unphysical “thresholds” $Q^2 = m^2$. From there one proceeds to their renormalization group evolution with an increased number of flavors $n = 4, 5$ and (eventually) 6.

For situations where the (threshold) invariant mass of the produced system far exceeds the mass of the interacting heavy flavor in the FFNS, the VFNS predictions have been shown [30] to deviate from the FFNS typically by about 10%, although the exact amount depends on the particular process and energy scale. This is usually within the margins of the renormalization and factorization scale uncertainties and other theoretical ambiguities related to PDFs. Eventually, one nevertheless has to *assume* that these massless “heavy” quark distributions are relevant asymptotically, in that they can correctly describe the relevant cross sections at scales much larger than the heavy quark masses involved.

Unfortunately this is not the case for DIS structure functions, for which the strictly massless approach, known in this context as the zero-mass VFNS, or ZM-VFNS, is well known to be experimentally inadequate, particularly near the heavy quark production thresholds. To remedy this the heavy-quark mass effects are re-inserted in what are known as general-mass VFNSs (GM-VFNS), for which several prescriptions are available in the literature [29, 31, 32, 33, 34] (see also Ref. [35]). These schemes interpolate (in a model-dependent way) between the FFNS results near production threshold and the asymptotic results of the ZM-VFNS. However, since the interpolating schemes are based on the same massive matrix elements as the FFNS, they do not have complete information on the $\mathcal{O}(\alpha_s^3)$ heavy flavor Wilson coefficients (even though they are sometimes referred to as “NNLO GM-VFNSs”).

The importance for global PDF analysis of finite heavy quark mass effects in the calculation of DIS structure functions had been previously emphasized in

Refs. [36, 37, 38], but was only universally recognized after the analysis of [39]. Currently the ABM [40] and JR [41, 42] collaborations use the FFNS for the calculation of DIS structure functions in their global analyses, while the MSTW [43], CT [44, 45], HERAPDF [46] and NNPDF [47] groups use variants of GM-VFNS. The calculations of hadron collider cross sections are carried out in the VFNS in all cases.

2.5. Power corrections

The elegant machinery that has been developed within the framework of perturbative QCD to analyze leading twist PDFs is, strictly speaking, valid only at high values of Q^2 and W where all hadron mass scales are suppressed, $M^2/Q^2, M^2/W^2 \ll 1$. In real experiments performed at a finite beam energy E , however, the maximum values of Q^2 and W are limited, which inevitably restricts the available coverage in Bjorken x . This is especially relevant at large x , where in DIS the invariant mass squared of the produced hadronic system is given by

$$W^2 = M^2 + Q^2 \left(\frac{1-x}{x} \right), \quad Q^2 < Q_{\max}^2 = 2ME x, \quad (27)$$

with M the mass of the target nucleon. For fixed Q^2 , as $x \rightarrow 1$ the final state hadron mass W decreases as one descends into the region dominated by nucleon resonances at $W \lesssim 2$ GeV. The resonance region may be treated using the concept of quark-hadron duality [48], although this goes beyond the scope of the usual pQCD analysis.

In the region of low Q^2 , power corrections to the Bjorken limit results that scale as powers of $\Lambda_{\text{QCD}}^2/Q^2$ become increasingly important. In the operator product expansion, these are associated with higher twist corrections, which arise from multi-parton correlations and characterize the long-range nonperturbative interactions between quarks and gluons. Of tremendous interest in their own right as providing glimpses into the dynamics of quark confinement, the power corrections are viewed as troublesome backgrounds to efforts aimed solely at extracting leading twist PDFs.

To avoid the complications from the higher twist corrections, the usual strategy in global PDF analyses is to apply cuts specifying minimum values of Q^2 and W^2 . In many analyses of unpolarized scattering data, the cuts are of the order $Q^2 \gtrsim 4$ GeV² and $W^2 \gtrsim 14$ GeV² [43, 44, 46, 47, 49], which in practice restrict the range of x that can be accessed to $x \lesssim 0.7$. For spin-dependent PDFs, the scarcity of high-energy data forces most global analyses to use less restrictive cuts, of the order $Q^2 > 1$ GeV² and $W^2 \gtrsim 4$ GeV². On the other hand, there are a number of important reasons for needing to know the large- x behavior of PDFs, and several recent unpolarized PDF analyses [40, 50, 51, 52, 53] have been performed with relaxed cuts of $Q^2 \gtrsim (1.3 \text{ GeV})^2$ and $W^2 > 3$ GeV² which have allowed an expanded reach into large x . The improvement in the large- x kinematic coverage amounts to about 1300 more data points for proton and deuteron targets, representing some $\sim 50\%$ increase in the total number of DIS data points compared with the more restrictive cuts. Most importantly, the resulting

leading twist PDFs fits have proved to be very stable even when such low cuts have been applied [51].

With the inclusion of the kinematic regions in which subleading $1/Q^2$ effects play a non-negligible role, it is obviously crucial to account for the power corrections that might otherwise obfuscate the leading twist PDFs. Among the different categories of $1/Q^2$ effects, the simplest are the target mass corrections (TMCs), which are formally associated with matrix elements of leading twist operators [54, 55, 56, 57] and are of kinematical origin. Others include genuine higher twist corrections, which arise from dynamical, multi-parton correlations, as well as higher order perturbative QCD corrections, which can also resemble power suppressed contributions at low Q^2 .

The standard method to compute TMCs in DIS is based on the operator product expansion, and was first formulated by Georgi and Politzer [54], and expressions for all unpolarized and polarized structure functions now exist in both x and Mellin space [55, 56, 57, 58, 59]. An alternative method based on collinear factorization (CF) in momentum space was developed by Ellis, Furmanski and Petronzio [60], and extended by various authors [58, 61, 62] (see also the recent reviews of TMCs in Refs. [64, 65]). The advantage of the OPE method is that TMCs can be calculated to all orders in $1/Q^2$ in DIS, whereas TMCs in the CF approach have only been computed to $\mathcal{O}(1/Q^2)$. On the other hand, the OPE is limited to inclusive DIS, while the CF framework can be applied to computing TMCs also in other processes [62]. Since typically the non-DIS data are taken at very high Q^2 where TMC effects are very small, the OPE method is usually adopted.

All of the TMC methods also suffer to some extent from the threshold problem, whereby the target mass corrected structure function remains nonzero as $x \rightarrow 1$ [59, 66, 67]. For the purposes of global fits, however, the region where the threshold effects become problematic is $W < 2$ GeV [59], which is mostly outside of where even the most liberal cuts in W and Q^2 are made [50, 51, 52]. From the seminal work of De Rújula *et al.* [68, 69], the appearance of the threshold problem in the analysis of TMCs is attributed to the neglect of dynamical higher twist corrections, both of which scale as powers in $1/Q^2$. (In fact, higher order perturbative QCD corrections can also resemble power suppressed contributions at low Q^2 .)

Regardless of their origin, the various power suppressed corrections that are not included in a leading twist calculation can be absorbed into phenomenological functions; for example, for an unpolarized structure function F_i ,

$$F_i(x, Q^2) = F_i^{\text{LT}}(x, Q^2) + \frac{h_i(x, Q^2)}{Q^2} + \frac{h'_i(x, Q^2)}{Q^4} + \dots, \quad (28)$$

where F_i^{LT} denotes the leading twist contribution including TMCs. The higher twist corrections are sometimes assumed to be multiplicative, with the functions h_i, h'_i proportional to the leading twist contribution, $h_i(x, Q^2) = F_i^{\text{LT}}(x, Q^2) c(x)$. Possible additional Q^2 dependence of the higher twist contributions, from radiative $\alpha_s(Q^2)$ corrections, is usually neglected. The leading twist PDFs were found in Ref. [51] to be essentially independent of the TMC prescription adopted, with the HT parameters

able to compensate for the variations due to the different TMC formulations. The isospin dependence of the HT corrections was also studied in Refs. [70, 71, 72, 73]. Existing data do not allow for an accurate determination of the $\mathcal{O}(1/Q^4)$ corrections h'_i , and attempts to include them in global fits produce anomalously small values of χ^2 and $\alpha_s(M_Z^2)$ in conjunction with large compensating twist-4 and twist-6 contributions [73, 74], possibly due to overfitting and blurring of the scaling violations.

In the polarized case, the greater scarcity of data means that typically one cannot afford the luxury of Q^2 and W cuts as stringent as those applied in some of the unpolarized PDF analyses. Most global analyses of spin-dependent PDFs therefore include structure function measurements down to $Q^2 = 1 \text{ GeV}^2$, where higher twist corrections are believed to be important. The higher twist contributions to g_1 and g_2 may be treated in an analogous way to the unpolarized F_i structure functions, with the important difference that the twist-3 contributions to g_2 are not Q^2 -suppressed. Phenomenological PDF analyses exist which include HT contributions to g_1 [75, 76], g_2 [77, 78], and to both functions simultaneously [79]. While the focus in the present work is on the leading twist PDFs, the higher twist contributions to g_1 and g_2 are also of intrinsic interest in themselves, containing information, for example, about the correlations of color electric and magnetic fields in the nucleon with the nucleon's spin [80, 81, 82, 83, 84].

2.6. Nuclear corrections

Since nucleons bound in a nucleus are not free, the parton distributions f_i^A in a nucleus A deviate from a simple sum of PDFs in the free proton and neutron, $f_i^A \neq Z f_i^p + (A-Z) f_i^n$, where Z is the number of protons. This phenomenon is especially relevant at small values of x , where nuclear shadowing (or screening) effects suppress the nuclear to free isoscalar nucleon (N) ratio, $f_i^A/(A f_i^N) < 1$, and at large x , where the effects of Fermi motion, nuclear binding, and nucleon off-shellness give rise to the ‘‘nuclear EMC effect’’ [85, 86, 87]. In addition, for spin-dependent PDFs, the different polarizations of the bound nucleons and nuclei need to be taken into account.

In the nuclear impulse approximation, where scattering is assumed to take place incoherently from partons inside individual nucleons, the PDF in a nucleus can be expressed as a convolution of the PDF in a bound nucleon and a momentum distribution function $\varphi_{N/A}$ of nucleons in the nucleus [88, 89, 90]. Coherent rescattering effects involving partons in two or more nucleons give rise to nuclear shadowing corrections to the impulse approximation. In general, at large Q^2 the PDFs in a nucleus and in a nucleon are related by

$$f_i^A(x, Q^2) = \sum_{N=p,n} \int \frac{dz}{z} \varphi_{N/A}(z) f_i^N(x/z, Q^2) + \delta^{(\text{off})} f_i^A(x, Q^2) + \delta^{(\text{shad})} f_i^A(x, Q^2), \quad (29)$$

where the additive term $\delta^{(\text{off})} f_i^A(x, Q^2)$ represents nucleon off-shell or relativistic corrections, and $\delta^{(\text{shad})} f_i^A(x, Q^2)$ parametrizes the shadowing corrections. A similar

expression can be written for spin-dependent PDFs.

The momentum distribution, or “smearing function”, $\varphi_{N/A}$, can be computed from nuclear wave functions, incorporating nuclear binding and Fermi motion effects. At $Q^2 \rightarrow \infty$ the smearing function has a simple probabilistic interpretation in terms of the light-cone momentum fraction $z = (M_A/M)(p \cdot q/P_A \cdot q) \approx (M_A/M)(p^+/P_A^+)$ of the nucleus carried by the struck nucleon, where p and P_A are the four-momenta of the nucleon and nucleus, respectively, and M_A is the nuclear mass. In this case the smearing function is normalized to unity, $\int dz \varphi_{N/A}(z) = 1$. At finite Q^2 , however, the smearing function depends in addition on the parameter $\gamma^2 = \mathbf{q}^2/\nu^2 = 1 + 4x^2M^2/Q^2$, where ν and \mathbf{q} are the energy and three-momentum transfer, respectively, which characterizes the deviation from the Bjorken limit [90, 91]. Typically, the function $\varphi_{N/A}$ is steeply peaked around $z \approx 1$, becoming broader with increasing mass number A as the effects of binding and Fermi motion become more important. In the limit of zero binding, $\varphi_{N/A}(z) \rightarrow \delta(1-z)$, and one recovers the free-nucleon case. This is the usual assumption made in most global PDF analyses.

Recently, several analyses [40, 50, 51, 52, 53] have accounted for the nuclear effects by explicitly calculating the corrections from microscopic nuclear models, or attempted to constrain them phenomenologically [92]. The most straightforward calculation is for the simplest nucleus — the deuteron, for which both nonrelativistic and relativistic wave functions are available [93, 94, 95], constrained by high-precision nucleon-nucleon scattering data. Experiments with deuterium targets play a vital role, in fact, in determining the flavor decomposition of the proton PDFs. Traditionally, the standard method for disentangling the u and d PDFs has been through charged lepton DIS, which for a proton target is sensitive at large x to the combination $4u + d$. DIS from a neutron would constrain $4d + u$; however, the absence of free neutron targets has necessitated the use of deuterium as effective neutron targets. While the nuclear corrections in the deuteron are typically a few percent, in some regions of kinematics, most notably at large x , they can give rise to large uncertainties in the extracted d quark PDF in particular.

An alternative, purely phenomenological approach [96] has attempted to constrain the nuclear corrections in deuterium directly from the data. However, without an independent, high-precision measurement of the d quark PDF from processes other than inclusive DIS, it is difficult to unambiguously separate the effects of the nuclear corrections from uncertainties in the d quark PDF, especially at high values x . Until future experiments (see Ref. [52] for a discussion) are able to determine the d quark PDF independent of uncertainties in nuclear models, a more practical approach adopted by the CJ Collaboration [53] has been to produce a set of global PDFs for a range of nuclear models, corresponding to mild (CJ12min), medium (CJ12mid), and strong (CJ12max) nuclear corrections in the deuteron.

The current uncertainties in PDFs from nuclear corrections can have important consequences far beyond the fixed-target experiments where they are encountered most directly. In fact, the effects of the nuclear smearing corrections are not suppressed at large Q^2 , and must be considered at all scales wherever data at $x > 0.5$ are used

[51, 97, 98]. Through Q^2 evolution, PDFs at large x and small Q^2 evolve to lower x and higher Q^2 , so that large- x uncertainties in fixed-target experiments can have significant consequences for collider measurements [99], examples of which were discussed for selected observables at the Tevatron and LHC in Ref. [100].

For neutrino scattering, in order to increase the relatively low rates and obtain sufficient statistics, experiments have often resorted to using heavier nuclear targets, such as iron or lead. This is particularly relevant for determinations of the strange quark PDF, which is typically extracted from opposite-sign dimuon events in ν and $\bar{\nu}$ charm production, $W^+ + s \rightarrow c$ or $W^- + \bar{s} \rightarrow \bar{c}$ [101, 102]. Such extractions are complicated by the presence of nuclear corrections in neutrino structure functions [90, 103], as well as effects of the nuclear medium on the charm quark propagation in the final state [63]. Uncertainties in the strange quark PDF can have significant impact on W and Z boson measurements at the LHC, for example, so that understanding of the nuclear effects will have impact far beyond lepton–nucleus DIS [104].

In order to systematically study the nuclear dependence of PDFs, without assuming specific relations between PDFs in nuclei and nucleons, several groups have parametrized nuclear PDFs directly [104, 105, 106, 107]. One approach has been to parametrize the A dependence of the initial proton PDF parameters, and then perform a global fit of the available hard scattering data on nuclear targets. This implicitly assumes a smooth A dependence for the PDFs, which is reasonable for large A , but may break down for light nuclei such as deuterium. An alternative method is to fit to one type of data set and examine how the results differ from those on proton targets. This can be useful for testing whether the nuclear corrections are consistent with those obtained from various data sets. Such comparisons have revealed, for instance, a controversy about whether or not the A dependence of the neutrino-nucleus data from the NuTeV collaboration is compatible with that observed in charged lepton DIS [107, 108, 109]. Differences between neutrino and electromagnetic nuclear interactions can arise, for instance, from the presence of the parity-odd F_3 structure function in $\nu/\bar{\nu}$ scattering, which does not contribute to charged-lepton scattering [103].

For spin-dependent scattering, the scarcity of data and their larger uncertainties at very small x and at high x , where nuclear corrections are most prominent, has meant that almost all global analyses have thus far relied exclusively on the effective polarization *ansatz*, in which the polarized PDF in the nucleus Δf_i^A is related to the polarized PDFs in the proton and neutron as $\Delta f_i^A \approx \langle \sigma \rangle^p \Delta f_i^p + \langle \sigma \rangle^n \Delta f_i^n$, with $\langle \sigma \rangle^{p(n)}$ the average polarizations of the proton (neutron) in the nucleus. In practice, only polarized deuterium and ^3He nuclei have been used in DIS experiments, in addition to protons. The new global analysis of helicity PDFs by the JAM collaboration [79] is the first systematic attempt to incorporate the effects of nuclear smearing in DIS structure functions of the deuteron and ^3He . This will be important as future spin-dependent scattering experiments probe the nucleon spin structure at increasingly large values of x [110, 111, 112, 113].

2.7. PDF parametrizations and sum rule constraints

The concept of global fitting for PDFs relies on the formalism outlined in the previous sections. Partonic cross sections for various hard scattering processes are convoluted with scale-dependent PDFs to generate results for physical observables which can then be compared to data. The PDFs are parametrized at some convenient input scale Q_0 and then evolved using the appropriate evolution equations to the scales needed for each calculation. The values of the input parameters are estimated using a χ^2 minimization technique. All of the global PDF fitting groups use some variation of this technique. A typical parametrization at the input scale Q_0 for a generic polarized or unpolarized parton (quark, antiquark or gluon) distribution function f is

$$xf(x, Q_0^2) = a_0 x^{a_1} (1-x)^{a_2} P(x), \quad (30)$$

where $P(x)$ represents some smoothly varying function usually chosen as a polynomial in x or \sqrt{x} , although exponential functions are used as well. In addition, there are parametrizations inspired by a statistical model of the nucleon [114], as well as those based on neural networks [115] and self-organizing maps [116].

Some of the parameters in the input distributions can be determined from physical constraints. For example, in the unpolarized case valence quark number is conserved,

$$\int_0^1 dx (q(x, Q_0^2) - \bar{q}(x, Q_0^2)) = \begin{cases} 2 & q = u, \\ 1 & q = d, \\ 0 & \text{otherwise,} \end{cases} \quad (31)$$

while the momentum sum rule requires

$$\int_0^1 dx x \left[\sum_q^{n_f} q^+(x, Q_0^2) + g(x, Q_0^2) \right] = 1, \quad (32)$$

where we use the notation $q^+ \equiv q + \bar{q}$, and the number of flavors at the input scale Q_0^2 is usually taken to be $n_f = 3$ (see Sec. 2.4). In the polarized case the first moments of the charge-conjugation even (or C -even) distributions can be related to octet baryon weak decay constants. For the isovector combination, corresponding to the Bjorken sum rule,

$$\int_0^1 dx (\Delta u^+(x, Q_0^2) - \Delta d^+(x, Q_0^2)) = g_A, \quad (33)$$

where $g_A = 1.270 \pm 0.003$ is the nucleon axial charge, while for the SU(3) octet one has

$$\int_0^1 dx (\Delta u^+(x, Q_0^2) + \Delta d^+(x, Q_0^2) - 2\Delta s^+(x, Q_0^2)) = a_8, \quad (34)$$

where the octet axial charge $a_8 = 0.58 \pm 0.03$ is extracted from hyperon β -decays assuming SU(3) flavor symmetry [117]. Note that the sum rules (31)–(34) are preserved under Q^2 evolution.

While most of the PDF groups use similar procedures and data, one can nevertheless obtain PDF results that can be rather different. Some of the reasons for this include the following:

- Differences in the specific parametrizations and input scale Q_0^2 .
- Differences in data selection, choices of data sets, kinematic cuts, and the specific treatment of the correlated errors of the data. This typically limits the amount of data available at large values of x .
- Differences in the theoretical framework used, including the particular form of the solutions of the RGE employed, the treatment of heavy quarks, inclusion of higher twist contributions, target mass effects, and nuclear corrections.

These differences should be born in mind when comparing the results from different PDF groups.

2.8. PDF errors

PDFs are an essential ingredient for producing predictions for processes in high energy experiments. The uncertainties in these predictions depend, in part, on how well determined the PDFs are themselves. It is important to bear in mind that the predictions that are compared to data are convolutions of PDFs with partonic hard scattering cross sections. There are thus three main sources of PDF uncertainties: the fitted data, the partonic cross sections, and the parametrizations used to describe the PDFs. The following list describes the main sources of uncertainty in the determination of PDFs.

- The experimental errors on the fitted data can be directly propagated to the fitted PDFs. Standard techniques include the Hessian [118], Lagrange [119], and Monte Carlo [120] methods.
- Uncertainties due to the use of perturbation theory: These can be estimated to some extent by doing LO, NLO, and NNLO fits, although not all processes are known to NNLO accuracy.
- Scale dependence: The perturbative predictions depend to some extent on the choices made for the renormalization and factorization scales for each process. These choices will change the results for each process and the fitted PDFs must compensate these changes (see Sec. III of Ref. [121] for an example of the effects of choosing different scales).
- Choice of the value of the running coupling $\alpha_s(M_Z)$: some PDF determinations fit $\alpha_s(M_Z)$ while others use the global average value. This is mostly a question of philosophy. On the one hand, since the strong coupling is a parameter of QCD, then there is no freedom to choose a different value for each process. Thus, information from data types not included in the global fits (such as data from e^+e^- processes) provides valid constraints on the value of the coupling and are included in determining the global average. On the other hand, fitting the value of the strong coupling and comparing it to the global average provides an interesting consistency check on the description of the data provided by QCD.

- Choice of data sets and kinematic cuts: these choices can affect the fitted PDFs and the user should be aware of these differences.
- Treatment of heavy quarks: the various schemes that are currently used differ at higher orders and such differences can affect the fitted PDFs.
- Parametrization dependence: fitted PDFs can differ simply through the choice of the initial parametrizations. Extensive efforts are made to choose flexible parametrizations which are well-constrained by data, but there is no control over the behavior outside the kinematic region covered by the data. This can lead to different extrapolations at very large or very small values of x . A method for estimating this remaining uncertainty has been suggested in Ref. [122].

Of all these sources of error, the easiest to treat is the first — the propagation of the experimental errors.

2.8.1. Hessian method. The Hessian method is described in detail in Ref. [118]. The elements of the Hessian matrix are given by

$$H_{ij} = \frac{1}{2} \frac{\partial^2 \chi^2}{\partial a_i \partial a_j} \quad (35)$$

where a_i denotes the i^{th} PDF parameter. The Hessian matrix is generated during the actual minimization procedure and its inverse is the error matrix. The eigenvectors of the error matrix can then be used to define eigenvector parameter sets which, in turn, can be used to calculate error bands for the PDFs or for specific processes. One particular subtlety is that the error bands generally depend on a χ^2 tolerance. Mathematically, one expects the 1σ parameter errors to correspond to an increase of χ^2 by one unit from the minimum value. However, it has been suggested [123] that inconsistencies between different data sets may require a larger value to be used. This “ χ^2 tolerance” varies between groups and allowance must be made for this when comparing the resulting error bands.

2.8.2. Lagrange multiplier method. The Lagrange multiplier [119] method is useful when one wants to determine the PDF error on a specific observable X such as the cross section for W or Z production. Let χ_{global}^2 denote the χ^2 for the global data set. Then one minimizes the function

$$\Psi(a, \lambda) = \chi_{\text{global}}^2 + \lambda X(a), \quad (36)$$

where a denotes the set of PDF parameters and minimization is done for a range of values of λ . The end result is a relation between χ_{global}^2 and the value X of the chosen observable. Once one specifies the χ^2 tolerance, *i.e.*, the range of allowable χ^2 values, this maps out a range of values

$$X_0 - \Delta X \leq X \leq X_0 + \Delta X$$

where X_0 is the value of X at the global minimum.

2.8.3. Monte Carlo method. An alternative to the usual linear propagation of errors (Hessian method) which can be useful for minima that are not well behaved or defined, is the so-called Monte Carlo method. In order to propagate the experimental errors a number of ‘replica’ data sets are generated by using random numbers and the original errors to generate new data points [120]. These replica data sets are then fitted and the resulting replica PDF sets are treated using standard statistics; the central values are given by the average over replicas, and the uncertainties by the envelope of predictions.

2.9. Data types

The main motivation for pursuing global fitting as a technique for determining PDFs is that the use of a wide range of data types with different kinematic coverage places many constraints simultaneously on the PDFs. Each type of observable depends on a particular linear combination of PDFs or products of PDFs. Obtaining the best fit to all of the observables simultaneously has proven to be an efficient method for extracting PDFs. Nevertheless, it remains true that specific observables may be sensitive to a specific PDF or combination of PDFs. In this section some examples using simplified LO kinematics will be presented since these can be useful in understanding how PDF errors can be reduced by future measurements.

2.9.1. Unpolarized experiments. **Deep-inelastic scattering** experiments provide direct information on PDFs since both the structure functions and the cross sections depend linearly on the PDFs. The following list summarizes the main dependences.

- (i) Charged lepton neutral current measurements on a proton target constrain the combination

$$4u^+ + d^+ + s^+,$$

where we have assumed that only single photon exchange contributes (Z boson exchange involves a different linear combination of PDFs). At large values of x the antiquark PDFs become negligible leaving the combination $4u_v + d_v$. If one had a neutron target, then the linear combination would be

$$4d^+ + u^+ + s^+,$$

which becomes $4d_v + u_v$ at large values of x . Of course, neutron targets are not available, so deuterium is often used for this purpose requiring that nuclear corrections be made in order to extract the neutron target information as discussed in Sec. 2.6.

- (ii) Charged current neutrino interactions constrains the combinations

$$\sum_i (q_i \pm \bar{q}_i),$$

where the plus (minus) sign corresponds to $F_{1,2}$ (xF_3). The actual linear combinations depend on the type of target used; high statistics neutrino

experiments employ different types of heavy targets for which model-dependent nuclear corrections must be made. Note that one can, in principle, isolate specific combinations of q or \bar{q} PDFs, depending on the type of target used. A special case is provided by charm production in neutrino and antineutrino scattering as these are proportional to the s and \bar{s} PDFs, respectively. The experimental signal is the production of opposite sign muon pairs requiring one to take into account the charm fragmentation and decay as well as nuclear corrections, depending on the type of target employed.

- (iii) The gluon PDF enters in DIS at $\mathcal{O}(\alpha_s)$. Thus, it is mainly constrained through the Q^2 dependence of the structure functions and Rosenbluth (or longitudinal/transverse) separated F_L data (see Sec. 3.6).

Vector boson production (lepton pairs, W^\pm , and Z^0) in LO proceed through $q\bar{q}$ annihilation. A few key examples are:

- (i) Lepton pair production in proton–proton and proton–neutron collisions depend on the combinations

$$\begin{aligned}\sigma^{pp} &\sim 4u(x_a)\bar{u}(x_b) + d(x_a)\bar{d}(x_b) + (x_a \leftrightarrow x_b) + \dots \\ \sigma^{pn} &\sim 4d(x_a)\bar{d}(x_b) + u(x_a)\bar{u}(x_b) + (x_a \leftrightarrow x_b) + \dots\end{aligned}$$

where $x_{a,b} = (M_B/\sqrt{s})e^{\pm y}$, and the \dots indicate contributions from the s , c and b quarks. Of course, the pn cross section is obtained from data from a deuterium target. These cross sections can be used to constrain the \bar{d}/\bar{u} ratio, for example.

- (ii) W^\pm production constrains products of the form $q\bar{q}'$ with specific weights given by the appropriate CKM matrix elements, whereas Z^0 production constrains $q\bar{q}$. For $p\bar{p}$ collisions at the Tevatron at large values of rapidity, one has approximately,

$$\begin{aligned}\sigma^{W^+} &\sim u(x_a)d(x_b) + \bar{d}(x_a)\bar{u}(x_b) + \dots \\ \sigma^{W^-} &\sim d(x_a)u(x_b) + \bar{u}(x_a)\bar{d}(x_b) + \dots\end{aligned}$$

where a (b) denotes the proton (antiproton), and the \dots represents contributions from heavier quarks. Note that these results are written in terms of proton PDFs. If the rapidity is large and positive, then $x_a > x_b$ and one can neglect the antiquark terms so that these cross sections directly constrain the u and d PDFs. Due to the missing neutrino from the W decays, one cannot directly reconstruct the rapidity distributions. What is usually presented is the charged lepton rapidity asymmetry for W^\pm production. In this case the decay process means that the constraints on the PDFs are less direct, but such measurements still provide useful constraints on the d/u ratio at moderate values of x . Of particular interest is the model dependent determination of the W rapidity asymmetry by the CDF Collaboration [124], which directly constrains the d/u ratio at large values of x since the asymmetry is for the W and not the charged lepton from the decay.

- (iii) Recently the ATLAS Collaboration has presented an analysis [125] using W decay lepton and Z^0 rapidity distribution data which shows potential for constraining the

strange quark PDF. This analysis makes use of the fact that the Z^0 cross section receives a significant contribution from $s\bar{s}$ annihilation while the W cross sections help constrain the \bar{u} and \bar{d} PDFs.

The other major class of observables includes inclusive **jet or photon, dijet**, and **photon + jet production**. Each of these constrain products of PDFs summed over all flavors. Nevertheless, there are certain PDFs that can be constrained by these observables. This follows since the u and d PDFs are well constrained by the DIS data and the vector boson and lepton pair production data provide strong constraints on the \bar{u} and \bar{d} PDFs. Hence, these data have the greatest impact on the gluon distribution.

- (i) Direct photon production in LO has two subprocesses: $qg \rightarrow \gamma q$ and $q\bar{q} \rightarrow \gamma g$. Hence, this process was thought to be a good candidate for constraining the gluon, especially at fixed target energies where the available x_T range extended out to about 0.6. However, photons can also be created by bremsstrahlung from the charged quarks – often referred to as the fragmentation process. Indeed, one can define photon fragmentation functions to help describe this production component. It turns out that at fixed target energies this component receives very large soft gluon corrections, requiring threshold resummation techniques [126]. This, combined with some apparent disagreements between experimental data sets [127, 128] meant that photon production has not fulfilled the original promise of constraining the gluon PDF. Recently, however, an analysis [129] suggests that the use of *isolated* photon collider data may well help constrain the gluon PDF. The use of isolation cuts reduces the fragmentation contribution and the use of higher energy collider reduces the need for threshold resummation.
- (ii) High- p_T jet production has played a significant role in constraining the gluon PDF. Even though the quark and antiquark PDFs are well constrained by other types of data, there are still significant contributions from qg and gg subprocesses [121].
- (iii) Dijet production triple differential cross sections yield more information than single jet cross sections because the rapidity of the second jet is also constrained, thereby helping to constrain the momentum fractions of the PDFs. By tuning the rapidity ranges for the two jets one can explore different regions for these momentum fractions. An example is given in Ref. [121].
- (iv) Photon + jet production offers similar constraints, but now the subprocesses are weighted by the squared charge of the parton to which the photon couples.

2.9.2. Polarized experiments. As with unpolarized measurements, historically most constraints on spin-dependent PDFs have come from **polarized charged-lepton DIS** experiments.

- (i) In the one-photon exchange approximation, the difference of inclusive DIS cross sections for leptons polarized longitudinally with spin parallel and antiparallel to

the target hadron polarization measures C -even quark combinations Δq^+ . For proton targets, one has the combination

$$4\Delta u^+ + \Delta d^+ + \Delta s^+,$$

while for the neutron the combination would be

$$4\Delta d^+ + \Delta u^+ + \Delta s^+,$$

with contributions from heavy quark polarization expected to be negligible. In practice, polarized ^3He targets are usually used as effective sources of polarized neutron, since the neutron carries almost 90% of the spin of ^3He , while polarized deuterons, to which the proton and neutron spins contribute equally, are used to provide the isoscalar combination

$$5(\Delta u^+ + \Delta d^+) + 2\Delta s^+.$$

Because of the greater sensitivity of the proton g_1 structure function measurements to the polarized u quark PDF, and uncertainties associated with nuclear corrections when extracting the neutron from ^3He or deuterium data, the uncertainty on the Δd PDF is significantly larger at high x than on Δu .

- (ii) At NLO, the polarized gluon distribution Δg also enters in the g_1 structure function. The Q^2 evolution of the flavor singlet contribution to g_1 can then be used to constrain Δg , as for the unpolarized gluon PDF discussed above, although the constraints are weaker in the polarized because $\Delta g/g \ll 1$ at small x .

Semi-inclusive DIS provides additional independent combinations of spin-dependent PDFs that can be used to reconstruct individual quark and antiquark flavors.

- (i) Semi-inclusive production of hadrons h in the current fragmentation region, primarily pions or kaons, is proportional to products of spin-dependent PDFs and quark \rightarrow hadron fragmentation functions,

$$\sum_q e_q^2 \Delta q(x) D_q^h(z),$$

where z is the fraction of the quark's energy carried by the hadron h . The fragmentation functions D_q^h can be determined from other reactions, such as inclusive hadron production in e^+e^- annihilation. One can weight particular quark or antiquark flavors by selecting favored (such as $D_u^{\pi^+}$ or $D_d^{\pi^+}$) or unfavored ($D_d^{\pi^+}$ or $D_u^{\pi^+}$) fragmentation functions for specific hadrons (in this case $h = \pi^+$). Information on the polarized strange quark PDF Δs in particular can be obtained from data on K production.

- (ii) The polarized gluon distribution Δg can be constrained by semi-inclusive DIS data on charmed or high- p_T hadron production through the photon-gluon fusion process. Recently the analysis of this process has been performed at NLO, extending earlier LO extractions of Δg .

Inclusive particle production in **polarized proton–proton collisions** provides an additional method of determining spin-dependent sea quark and gluon distributions.

- (i) W^\pm production cross sections for scattering longitudinally polarized protons from unpolarized protons, $\vec{p}p \rightarrow W^\pm X$, depend on products of spin-dependent and spin-averaged PDFs, for example,

$$\begin{aligned}\Delta\sigma^{W^+} &\sim \Delta\bar{d}(x_a)u(x_b) - \Delta u(x_a)\bar{d}(x_b) \\ \Delta\sigma^{W^-} &\sim \Delta\bar{u}(x_a)d(x_b) - \Delta d(x_a)\bar{u}(x_b).\end{aligned}$$

At large positive or negative rapidities, $x_a \gg x_b$ or $x_a \ll x_b$, the cross sections (or asymmetries) are dominated by a single flavor, while at mid-rapidities both u and d flavors contribute.

- (ii) Inclusive jet or π^0 production in double-polarized proton–proton scattering, $\vec{p}\vec{p} \rightarrow \text{jet}/\pi^0 + X$, is sensitive to the polarized gluon PDF. The first evidence for a small, but nonzero Δg was recently observed by the STAR Collaboration at RHIC in jet data at $\sqrt{s} = 200$ GeV. Direct photon production in polarized pp scattering has also been suggested [130] as a means of probing Δg .

3. Unpolarized parton distributions

Using the technology outlined in Sec. 2, a number of global QCD analyses of the world’s high-energy scattering data have produced sets of proton PDFs, up to next-to-leading order (NLO) or next-to-next-to-leading order (NNLO) accuracy. The efforts have indeed been global, with groups in Europe and the US in the forefront of the data analyses. The PDFs sets include parametrizations from the MSTW [43] and ABM [40] groups, both of which use standard global fitting methodology; the NNPDF [49] collaboration, which uses a newer approach based on neural networks; the JR [42] PDFs, which are dynamically generated through Q^2 evolution from a low Q^2 input scale; and the HERAPDF [46] group, which includes only data from the H1 and ZEUS experiments at HERA. The US-based efforts have been centered around the CTEQ Collaboration [131], which at present involves two derivative analyses of nucleon PDFs, by the CT [44] and CJ (CTEQ-Jefferson Lab) [53] groups, as well as the nCTEQ [104, 107] analysis of nuclear PDFs. The CJ Collaboration in particular has focused on developing the methodologies needed for describing data over a broad energy range including the low- Q^2 and W domain [51].

In this section we summarize the results for unpolarized PDFs from the various PDF fitting groups, discussing their similarities and contrasting their differences. We will focus mostly on the physics issues, rather than on technical aspects of PDF fitting. Of course with new data arriving or soon anticipated at the LHC, Jefferson Lab, and other facilities, the global fitting efforts are constantly evolving, so that the information presented here can only be viewed as a snapshot of the field at the present time.

As a typical example of modern PDFs and their uncertainties, Fig. 1 shows the xu , xd , $x(\bar{d} + \bar{u})$, $x(\bar{d} - \bar{u})$, xs and xg PDFs (with the gluon scaled by a factor 1/10) for

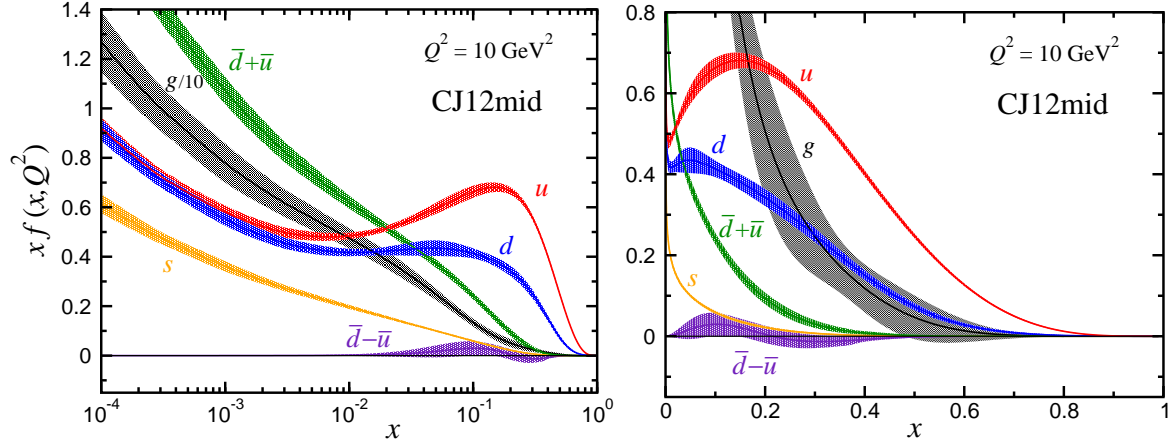


Figure 1. Uncertainty bands for the xu (red), xd (blue), $x(\bar{d} + \bar{u})$ (green), $x(\bar{d} - \bar{u})$ (violet), xs (orange) and xg (black) PDFs for the CJ12mid fit [53] at $Q^2 = 10 \text{ GeV}^2$, shown on logarithmic (*left*) and linear (*right*) scales in x . Note that in the left panel the gluon is scaled by a factor 1/10.

the CJ12 fit [53] (for the case of moderate nuclear corrections, CJ12mid) at a scale of $Q^2 = 10 \text{ GeV}^2$. The general behavior of the PDFs is similar for all the parametrizations [42, 40, 43, 44, 46, 49, 53], particularly where sufficient data exist to constrain the distributions in specific regions of x and Q^2 . In regions where data are scarce, such as at very low x ($x \lesssim 10^{-4}$) or high x ($x \gtrsim 0.4 - 0.6$) for certain observables, or where data on specific PDFs (such as the strange quark) are subject to large experimental or theoretical uncertainties, the details of the PDFs can depend strongly on the assumptions adopted in the extrapolations.

Some of these differences are evident in Figs. 2 and 3, which illustrate the flavor nonsinglet combinations $\{x(u - \bar{u}), x(d - \bar{d}), x(\bar{d} - \bar{u}), x(s - \bar{s})\}$, and the singlet-sector distributions $\{x(u + \bar{u}), x(d + \bar{d}), x(s + \bar{s}), xg\}$, respectively, for the NNLO MSTW08 [43], ABM11 [40], NNPDF [49] and JR09 [42] PDF sets. While the valence u_v and d_v PDFs are fairly well constrained in the intermediate- x region, at large x there are significant uncertainties on the d_v distribution in particular. The SU(2) nonsinglet distribution $\bar{d} - \bar{u}$ is well determined by data from the Drell-Yan reaction over the range $x \approx 0.05 - 0.25$, but is not constrained at higher x . The strange nonsinglet distribution is the most difficult to determine, requiring a combination of neutrino and antineutrino scattering data, which are subject to large experimental and nuclear uncertainties.

For the C -even distributions in Fig. 3, the $u + \bar{u}$ and $d + \bar{d}$ are the dominant quark distributions at large x , but the strange quark PDF becomes increasingly more important at small x . Numerically, the gluon distribution dominates all other PDFs at small x , but has sizable uncertainties at large x values. In the following sections we discuss features of each of the PDFs in more detail.

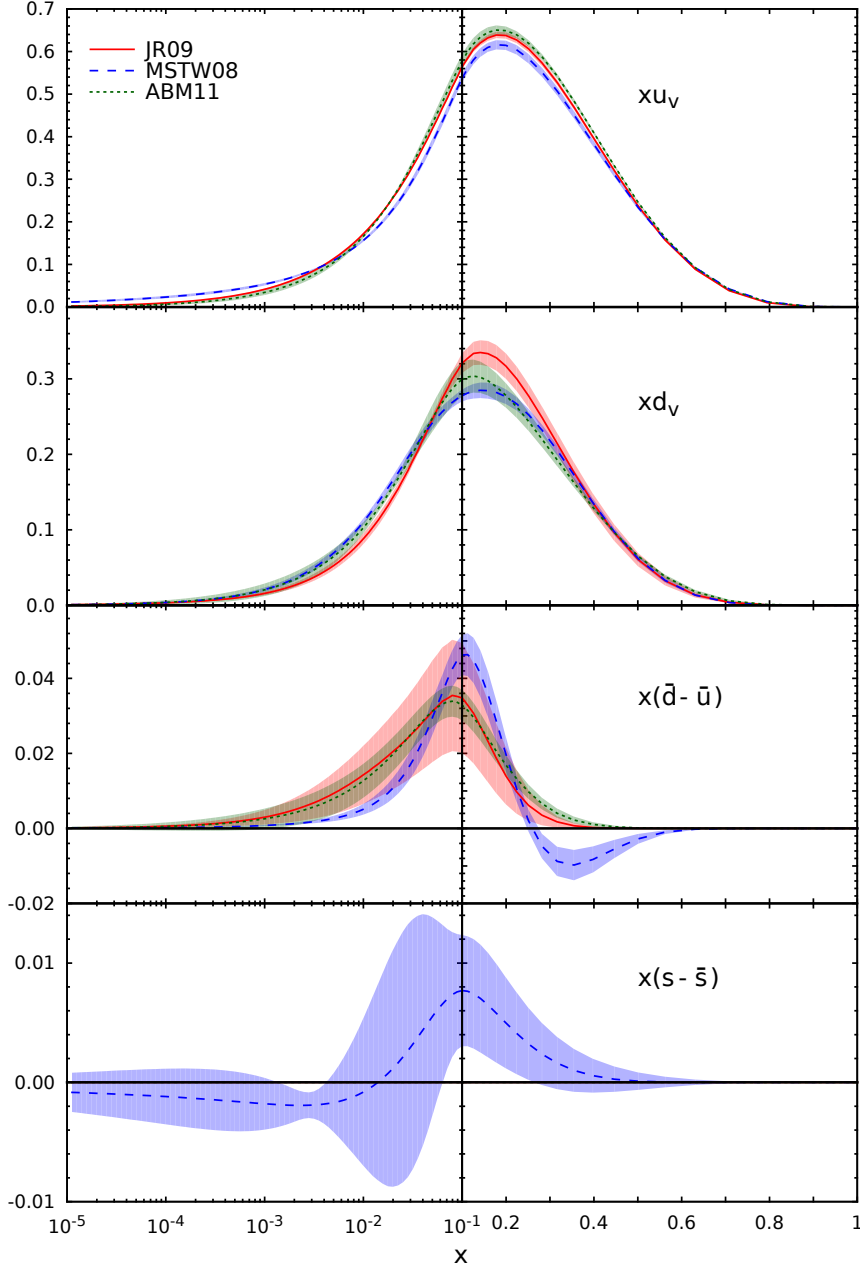


Figure 2. Comparison of nonsinglet PDF combinations, including the valence xu_v and xd_v , and the $x(\bar{d} - \bar{u})$ and $x(s - \bar{s})$ sea distributions, for the available 3-flavor NNLO PDF sets from JR09 [42] (red solid line), MSTW08 [43] (blue dashed) and ABM11 [40] (green dotted), at $Q^2 = 10 \text{ GeV}^2$.

3.1. Valence quarks at large x

Valence quarks give the global properties of the nucleon, such as its charge and baryon number. Knowledge of their momentum distributions is important for many reasons, especially at high values of x where a single quark carries most of the nucleon's momentum. The large- x region is in fact a unique laboratory for studying

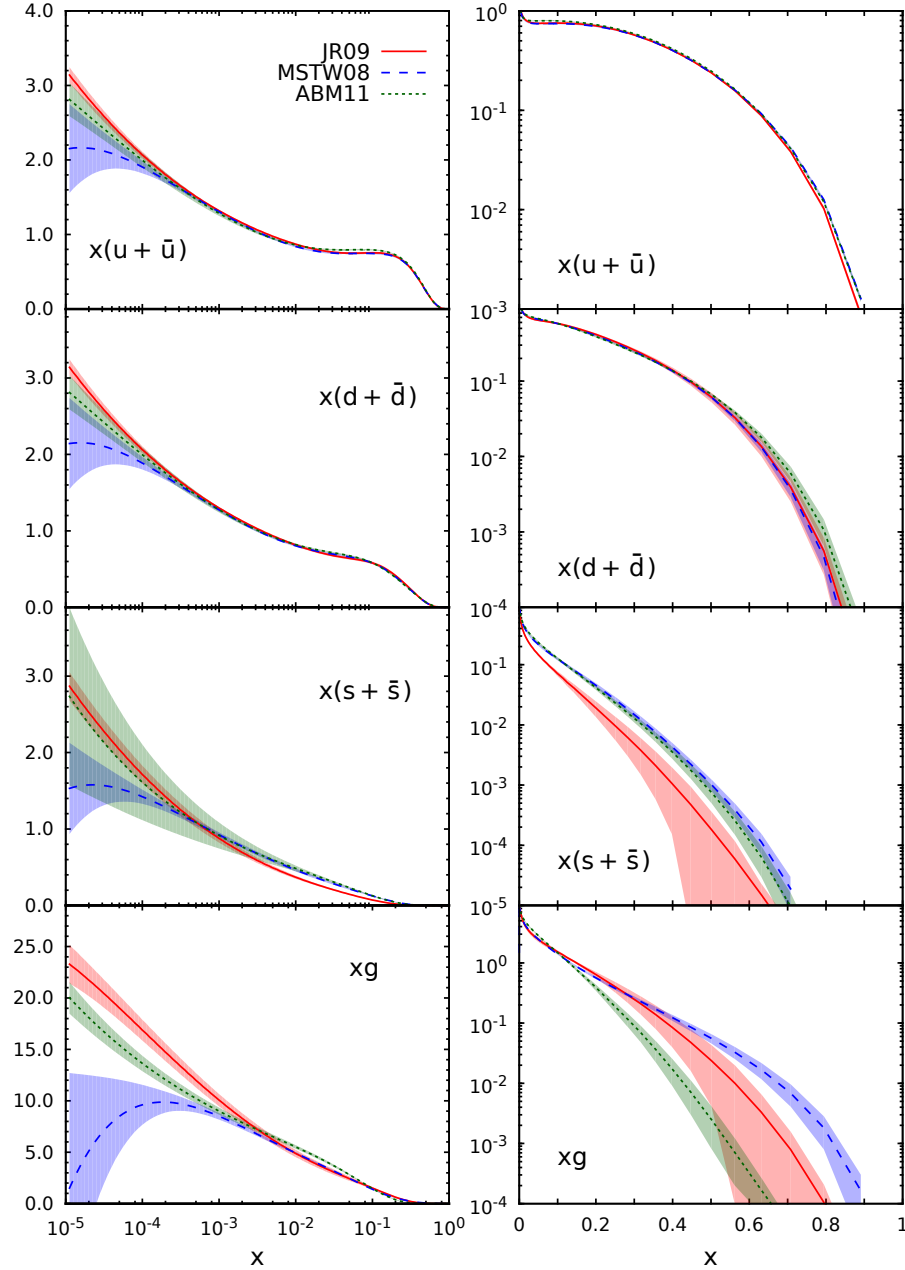


Figure 3. As in Fig. 2, but for the singlet-sector distributions $x(u + \bar{u})$, $x(d + \bar{d})$ and $x(s + \bar{s})$ and the gluon xg PDF.

the nonperturbative flavor and spin dynamics of quarks [132, 133, 134, 135], as well as testing predictions from perturbative QCD for the behavior of PDFs in the limit $x \rightarrow 1$ [136, 137, 138, 139].

Reliable determination of PDFs at large x is also important for searches for new physics beyond the Standard Model in collider experiments at the LHC. Through perturbative QCD evolution, uncertainties in PDFs from fixed-target experiments at high x and low Q^2 can propagate to larger Q^2 to affect cross sections at smaller x values

[99, 100]. This is especially true for the forward production of particles of mass m at large rapidities y , whose cross sections are given by products of PDFs with one evaluated at small $x \approx (m/\sqrt{s})e^{-y}$ and the other at large $x \approx (m/\sqrt{s})e^y$. The production of heavy W' and Z' bosons, for example, is sensitive to d quark PDF uncertainties at high rapidities, exceeding 100% in the W'^- channel, which places limits on the accuracy of cross section measurements for masses near the kinematic thresholds [100]. Furthermore, understanding PDFs at large x is vital for the analysis of neutrino oscillation experiments [140, 141, 142], where one of the most significant uncertainties comes from neutrino–nucleus cross sections at the interface of the DIS and resonance regions.

The growing need to better understand large- x PDFs and their uncertainties has been reflected in the greater attention being paid recently to the physics of the large- x region, with dedicated experiments planned at Jefferson Lab following its 12 GeV upgrade [143, 144, 145], as well as at proposed new facilities such as the LHeC [146] and the Electron-Ion Collider [113]. It has also been a catalyst for the recent concerted theoretical efforts by the CJ Collaboration [147] in their global QCD analyses of PDFs extending into the lower Q^2 and W^2 regions, with the aim of providing better constraints on PDFs at large values of x [51, 52, 53].

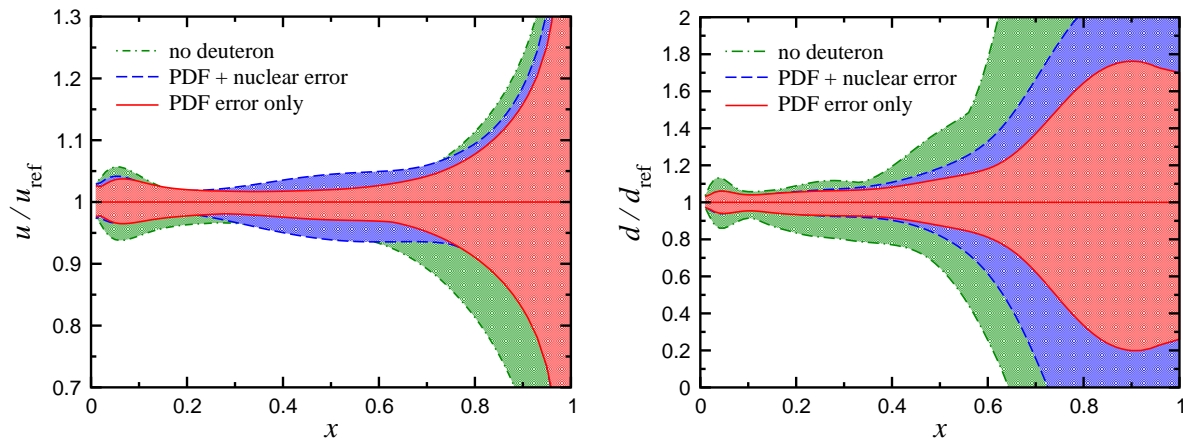


Figure 4. u and d quark distributions from the CJ12mid PDFs [53], with PDF errors only (solid, red shaded) with combined PDF and nuclear uncertainties (dashed, blue shaded), and with a fit excluding all deuterium data (dot-dashed, green shaded), relative to the reference CJ12mid set at an arbitrary scale $Q^2 = 100 \text{ GeV}^2$. Note the different vertical scales for the u and d quark PDFs.

The current constraints on the u and d quark distributions are illustrated in Fig. 4 for the CJ12mid PDF set [53], where the uncertainties arising from nuclear corrections and PDF (experimental) errors are indicated separately. Since the u quark PDF is relatively well constrained by the proton DIS data at large x , the effect of the nuclear uncertainties is minor, increasing the total uncertainty at intermediate x by a few percent. For the d quark distribution, on the other hand, whose determination at present requires both proton and deuterium DIS data, the nuclear correction uncertainties in

the deuteron significantly increase the overall error for $x \gtrsim 0.6$. However, even though the use of deuterium data introduces the need to confront the problem of nuclear effects and their uncertainties, without these data the error bands on the d quark PDF would be even larger over most of the x range, as Fig. 4 demonstrates.

In addition to accounting for the finite- Q^2 (TMC and higher twist) and nuclear effects which become increasingly important as x tends to 1 at fixed Q^2 , the behavior of PDFs in the $x \rightarrow 1$ limit also depends critically on the functional form used for the x dependence. The conventional parametrizations utilized in most global PDF analyses assume a $\sim (1-x)^{a_2}$ dependence for both the u and d quark PDFs, as in Eq. (30) above, so that in the limit as $x \rightarrow 1$, the d/u ratio tends either to zero or infinity. Accardi *et al.* [52] allowed for a more flexible parametrization of the valence d quark PDF, in which the d_v distribution receives a small admixture from the u_v PDF,

$$d_v \rightarrow d_v + b x^c u_v, \quad (37)$$

with b and c as free parameters. Provided the d quark has a softer momentum dependence (larger exponent a_2) than the u quark, which agrees with phenomenology, the ratio of the distributions will approach a constant value, $d_v/u_v \rightarrow b$, as $x \rightarrow 1$. A nonzero, finite value in this limit is in fact expected in several different nonperturbative models of nucleon structure [134, 135, 136].

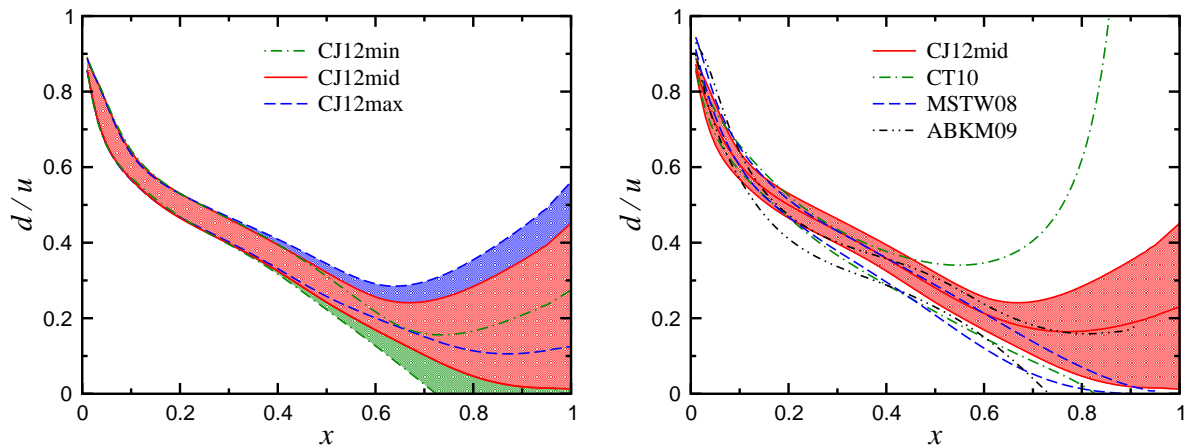


Figure 5. d/u ratio for the (left) CJ12min (dot-dashed), CJ12mid (solid) and CJ12max (dashed) PDFs [53], and (right) CJ12mid (solid) compared with the CT10 [44] (dot-dashed), MSTW08 [43] (dashed) and ABKM09 [50] (dot-dot-dashed) parametrizations at $Q^2 = 100 \text{ GeV}^2$.

The ratio of the d to u quark distributions is illustrated in Fig. 5 for several modern NLO PDF sets, including the CJ12 [53], CT10 [44], MSTW08 [43] (dashed) and ABKM09 [50] distributions. As expected, the total uncertainty on the d/u ratio at large x increases when different nuclear correction models are considered, with the central values extrapolated to $x = 1$ increasing from $d/u \approx 0$ for the CJ12min PDFs, with the minimum nuclear correction model, to $d/u \approx 0.3$ for the CJ12max set with the maximum nuclear correction model from Ref. [53]. Combining all uncertainties, the

CJ12 analysis found $d/u \rightarrow 0.22 \pm 0.20$ [PDF] ± 0.10 [nucl] as $x \rightarrow 1$, where the first error is from the PDF fits and the second is from the nuclear correction models.

In contrast, using the more restrictive, conventional parametrizations, the d/u ratios for the MSTW08 and ABKM09 distributions tend to zero in the $x \rightarrow 1$ limit, while that for CT10 tends to infinity. This behavior distorts somewhat the error bands, making the MSTW08 ratio appear to have an anomalously small uncertainty, while the CT10 result has a much larger one. The relative errors, however, are similar for the MSTW08 and CT10 PDFs, while the CJ12 and ABKM09 uncertainties are reduced at larger x because of the additional high- x data used in those analyses. Unfortunately, the extrapolated values of d/u at $x = 1$ span most of the range of available predictions [132, 133, 134, 135, 136], so that discrimination between the physical mechanisms that lead to the different $x \rightarrow 1$ behaviors will only be possible with constraints from new experiments that do not involve deuterium data and the nuclear model uncertainties [143, 144, 145].

3.2. Light quark sea

Inclusive electromagnetic DIS probes C -even combinations of PDFs, $q + \bar{q}$, weighted by their squared charges, or in terms of valence and sea quark (or antiquark) distributions, $q_v + 2\bar{q}$. The shapes of the quark valence and sea distributions differ markedly as a function of x . As we have seen in the preceding section, the valence quark PDFs dominate at intermediate and large values of x , but vanish as $xq_v \rightarrow 0$ for $x \rightarrow 0$. The sea, in contrast, dominates at small x , but is strongly suppressed as $x \rightarrow 1$. For the light antiquarks \bar{u} and \bar{d} , structure function data with proton targets are sensitive at small x to the combination $4\bar{u} + \bar{d}$, while deuterium targets (nuclear corrections aside) probe the isosinglet combination $\bar{u} + \bar{d}$. Under Q^2 evolution, the singlet quark distribution mixes with the gluon, which leads to the rapid growth in the antiquark PDFs with decreasing x . With increasing Q^2 , the uncertainties on $\bar{u} + \bar{d}$ also decrease.

Inclusive DIS measurements can therefore provide important constraints on the behavior of both the q_v and \bar{q} distributions in the regions where their contributions are dominant. However, in the intermediate- x region, $x \sim 0.01 - 0.1$, where the magnitude of valence and sea quark PDFs is comparable, additional information is required to uniquely determine the distributions individually. Here data from neutrino scattering can allow access to the parity-violating F_3 structure function, which measures C -odd combinations of PDFs, $q - \bar{q}$. Combined with the C -even PDFs from the parity-conserving F_1 and F_2 structure functions, one can then uniquely determine the q and \bar{q} distributions individually. Unfortunately, neutrino scattering cross sections are usually statistics limited compared with electromagnetic data, and with few exceptions, have necessitated the use of nuclear targets such as iron or lead as a means of increasing the rates. This subsequently brings with it the inherent complications associated with accounting for nuclear corrections in relating the nuclear structure functions with those in a free nucleon [90, 103].

More direct constraints on \bar{q} distributions can be obtained from lepton pair production in inclusive hadron–hadron scattering, which involves products of PDFs evaluated at different values of beam (x_a) and target (x_b) momentum fractions. As discussed in Sec. 2.3.2, the Drell-Yan process or W^\pm -boson production in pp scattering at nonzero rapidity, for example, allows the antiquark distribution at small x_a to be extracted with knowledge of the corresponding quark distribution at x_b .

In particular, the Drell-Yan reaction [148] has been used by the NA51 Collaboration at CERN [149] and the E866/NuSea Collaboration at Fermilab [150, 151] to determine the ratio of \bar{d} to \bar{u} distributions in the proton. Naive expectations from perturbative QCD based on $g \rightarrow q\bar{q}$ splitting suggest that since the masses of the u and d quarks are very similar, the production of $u\bar{u}$ and $d\bar{d}$ pairs should be nearly identical, even with the inclusion of higher-order radiative corrections [152]. The first indication of a significant asymmetry in the proton sea was obtained by the New Muon Collaboration (NMC) [153, 154] at CERN, who performed an accurate measurement of the ratio of DIS cross sections for hydrogen and deuterium, from which the Gottfried sum S_G was determined [155],

$$S_G = \int_0^1 \frac{dx}{x} (F_2^p - F_2^n) = \frac{1}{3} + \frac{2}{3} \int_0^1 dx (\bar{u} - \bar{d}), \quad (38)$$

where charge symmetry is assumed (see Sec. 3.3 below). For a flavor symmetric SU(2) proton sea, the prediction for the Gottfried sum would be $S_G = 1/3$. In contrast, the NMC measurement found $S_G = 0.235 \pm 0.026$ [154], indicating a strong violation of flavor symmetry in the light antiquark sea,

$$\int_0^1 dx (\bar{d} - \bar{u}) = 0.148 \pm 0.039. \quad (39)$$

Following the suggestion by Ellis and Stirling [156] that the light antiquark sea could be more directly probed in the Drell-Yan process, the NA51 experiment used the ratio of dimuon cross sections for pd and pp scattering to extract the ratio $\bar{d}/\bar{u} = 1.96 \pm 0.15 \pm 0.19$ at an average $\langle x \rangle = 0.18$ at a Feynman- x of $x_F = x_a - x_b \approx 0$. Subsequently, the E866/NuSea experiment at Fermilab measured the σ^{pd}/σ^{pp} ratio at large x_F , where at leading order

$$\frac{\sigma^{pd}}{2\sigma^{pp}} \approx \frac{1}{2} \left[1 + \frac{\bar{d}(x_b)}{\bar{u}(x_b)} \right], \quad x_a \gg x_b. \quad (40)$$

The results, illustrated in Fig. 6, confirmed a significant deviation of the cross section ratio from the naive perturbative QCD expectation, indicating a large asymmetry between \bar{d} and \bar{u} .

The earliest efforts to explain an enhancement of \bar{d} quarks over \bar{u} in the proton invoked the effects of Pauli blocking, which arise from the presence of different numbers of valence u and d quarks in the proton [157]. Estimates of this effect are very difficult to quantify reliably [158, 159], with some calculations [160] even suggesting that it produces a small excess of \bar{u} over \bar{d} . Alternative explanations have focused on the role of chiral symmetry breaking and the pion cloud of the nucleon [161]. Because of the Heisenberg

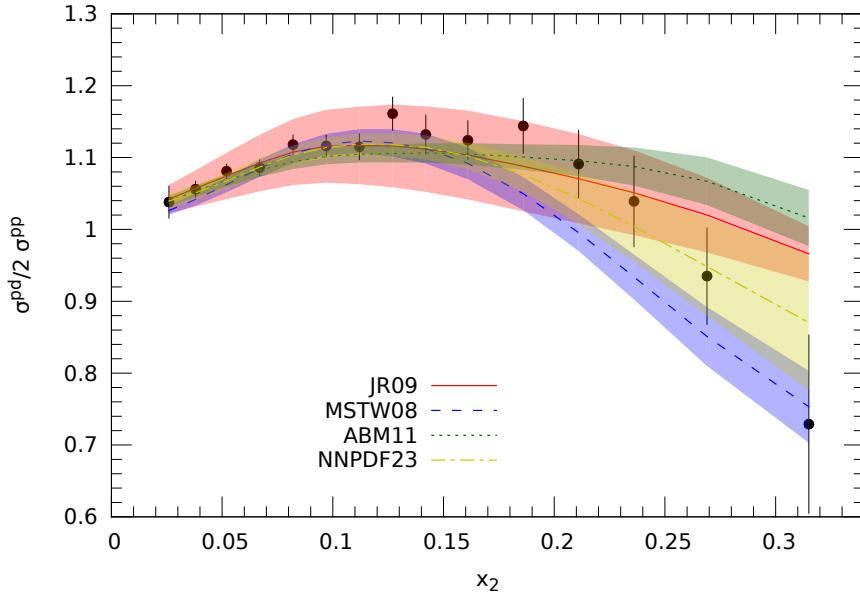


Figure 6. Ratio of lepton pair production cross sections in pd and pp scattering as a function of the fractional momentum x_b of the target parton. The data points from the Fermilab E866/NuSea Collaboration [151] are compared with the cross section ratio calculated using the JR09 [42] (red solid line), MSTW08 [43] (blue dashed), and ABM11 [40] (green dotted), and NNPDF23 [49] (yellow dot-dashed) PDF parametrizations.

uncertainty principle, a component of the proton’s wave function involves its dissociation into a nucleon and a virtual pion state. The preferential coupling of a proton to a $n\pi^+$, with the π^+ containing a valence $u\bar{d}$ pair, implies a natural mechanism for generating an excess of \bar{d} over \bar{u} . While many models have been proposed to compute this effect quantitatively (see Refs. [162, 163] for reviews), the underlying physics principles are model independent and simply the chiral symmetry properties of QCD [164, 165].

While most of the modern PDF parametrizations are able to accommodate an enhanced \bar{d} sea over the range $0.02 \lesssim x \lesssim 0.25$, there is some uncertainty in the trend of the \bar{d}/\bar{u} ratio at larger x . The new Drell-Yan experiment E906/SeaQuest at Fermilab [166] will extend the x coverage up to $x \approx 0.45$, and a proposal at the J-PARC facility in Japan [167, 168] would extend the range even further.

3.3. Charge symmetry violation in PDFs

Most PDF analyses have been performed under the assumption of charge symmetry, or independence of interactions under rotations in isospin space. Charge symmetry implies that the u quark distribution in the proton is identical to the d quark distribution in the neutron, and *vice versa*, and is believed to be accurate in nature at the $\lesssim 1\%$ level. This symmetry is broken explicitly by light quark mass differences, $m_u \neq m_d$, as well as by electromagnetic corrections. Such effects lead to nonzero values of the “majority”

and “minority” charge symmetry violating asymmetries in the nucleon, defined as

$$\delta u(x, Q^2) = u^p(x, Q^2) - d^n(x, Q^2), \quad (41)$$

$$\delta d(x, Q^2) = d^p(x, Q^2) - u^n(x, Q^2), \quad (42)$$

respectively, and similarly for the antiquarks $\delta\bar{q}$.

Although there is currently no direct evidence for charge symmetry violation (CSV) in PDFs, it has been predicted in several nonperturbative models for both valence and sea quark PDFs [169, 170, 171, 172]. In addition, electromagnetic radiative effects can be included in the Q^2 evolution equations (Sec. 2.2), in analogy with usual gluon radiation, by adding a term that accounts for the emission of photons by quarks [173, 174],

$$Q^2 \frac{\partial f_i(x, Q^2)}{\partial Q^2} = \sum_j \left(P_{ij}^{(\text{QCD})} \otimes f_j + P_{ij}^{(\text{QED})} \otimes f_j \right). \quad (43)$$

Here $P_{ij}^{(\text{QED})}$ are the new QED splitting functions (expanded in terms of the electromagnetic coupling α), and the sum over partons includes also the photon PDF $\gamma(x, Q^2)$. Even with charge symmetric PDFs at the input scale, the different electric couplings of the photon to u and d quarks in the modified evolution equations will induce nonzero CSV distributions (41) and (42) at a higher scale.

The valence quark asymmetries resulting from the QED-modified Q^2 evolution (43) are illustrated in Fig. 7 at a scale $Q^2 = 10 \text{ GeV}^2$. The perturbatively generated CSV distributions from Glück *et al.* [173] are calculated with an average isoscalar quark mass $m_q = 10 \text{ MeV}$, with the QED radiative corrections computed after fixing the QCD evolution effects. The majority valence δu_v distribution is negative at intermediate x values, and is of opposite sign to the minority valence distribution δd_v , which is smaller in magnitude. Qualitatively, these features are similar to the nonperturbative CSV valence asymmetries computed in the bag model [169, 170, 171], which arise from differences between the spectator uu and dd diquark masses, as well as the proton–neutron mass difference.

The MRSTQED [174] analysis of CSV was similar to that in Ref. [173], but involved unequal photon PDFs in the proton and neutron resulting from QED radiation with quark masses $m_{u(d)} = 6(10) \text{ MeV}$. Since the photon now also contributes to the momentum sum rule, Eq. (32), the CSV photon distributions induce charge symmetry violation in the valence quark PDFs, assuming the sea and gluon are charge symmetric. Despite the different assumptions, the resulting distributions turn out to be similar to those in Fig. 7.

While the overall magnitude of the possible CSV effects is rather small, they can nevertheless play an important role in understanding the discrepancy between the NuTeV measurement of $\sin^2 \theta_W$ [175] and the Standard Model value [9]. The NuTeV Collaboration extracted the Paschos-Wolfenstein (PW) ratio [176] of total neutral to charged current cross sections, involving the difference between ν and $\bar{\nu}$ cross sections. In addition to assuming small uncertainties on the nuclear corrections necessary for translating the measured iron target data to an isoscalar nucleon target, the analysis

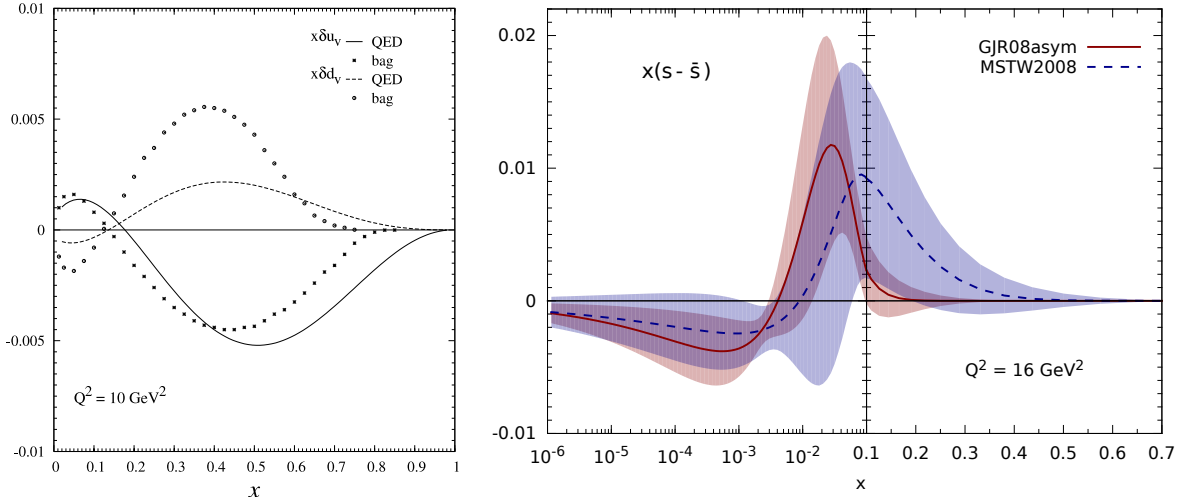


Figure 7. (Left) The CSV “majority” δu_v and “minority” δd_v valence quark distributions for the radiative QED fit of Ref. [173] at $Q^2 = 10 \text{ GeV}^2$, compared with the bag model estimates have been taken from Ref. [171]. (Right) Strange–antistrange asymmetry at $Q^2 = 16 \text{ GeV}^2$ (appropriate for the NuTeV experiment) for the asymmetric GJR08 [177] (red solid) and the MSTW2008 [43] (blue dashed) PDFs.

also neglected any CSV effects. Including CSV corrections, the experimental PW ratio would receive a contribution proportional to $\int_0^1 dx x (\delta d_v - \delta u_v)$ [172]. Depending on the sign of the CSV distributions, the asymmetry can therefore either remove some of the discrepancy with the NuTeV result, or exacerbate it. The signs and magnitude of the predicted perturbative QED and nonperturbative quark model asymmetries in Fig. 7 would in fact remove approximately 2/3 of the discrepancy.

An additional correction to the PW ratio can arise from differences between strange and antistrange distributions in the nucleon, $\int_0^1 dx x (s - \bar{s})$, which we discuss in the next section.

3.4. Strange quarks

Traditionally the strange quark distribution has been more difficult to determine experimentally than the non-strange sea. In practice one has often assumed that the s and \bar{s} PDFs (which are often assumed to be identical) are proportional to the $\bar{u} + \bar{d}$ distributions,

$$\kappa = \frac{s + \bar{s}}{\bar{u} + \bar{d}}, \quad (44)$$

with κ ranging between ~ 0.2 and 0.5 . The s and \bar{s} distributions can be directly determined, however, through the measurement of dimuon pairs in neutrino DIS, which are produced through the charged current by scattering from strange quarks with subsequent generation of charm. In particular, while neutrino scattering produces charmed hadrons ($W^+ s \rightarrow c$), antineutrino scattering results in anticharmed hadrons

($W^- \bar{s} \rightarrow \bar{c}$). The semileptonic decay of the charmed hadrons (such as D and \bar{D} mesons) then yields $\mu^+ \mu^-$ pairs along with the associated hadronic debris. Because of the low rates involved in neutrino scattering experiments, in order to increase the statistics these have typically made use of heavy nuclear targets, such as iron. Since the nuclear effects for neutrino and charged lepton scattering are in general different [103], the nuclear corrections introduce an additional source of uncertainty in extractions of the strange quark PDF.

A number of nonperturbative models have in fact predicted an asymmetry between the s and \bar{s} distributions in the nucleon, which can be probed by taking the difference between the ν and $\bar{\nu}$ cross sections. For example, in analogy with the pion cloud models invoked to explain the \bar{d} excess over \bar{u} in the proton in Sec. 3.2, the dissociation of a nucleon to a hyperon and a virtual kaon naturally produces unequal s and \bar{s} distributions, although the magnitude and even the sign is difficult to determine unambiguously [178, 179, 180, 181]. In addition, an asymmetry can also be generated through perturbative QCD evolution at NNLO because of unequal valence u and d distributions [182].

The CCFR [101] and NuTeV [102] collaborations at Fermilab have collected the highest statistics data on inclusive charm production in ν and $\bar{\nu}$ scattering on an iron target, enabling the most direct constraints to be placed on the strange quark PDFs as a function of x . The latter in particular was the first analysis using a complete NLO description of charm production. The cross section for (anti)neutrino charm production was computed to NLO in Refs. [183, 184] within the FFNS, in which, apart from the gluon, only the light quark flavors (u, d, s) are included as massless partons (see Secs. 2.4 and 3.5). The fully differential NLO calculation, including acceptance corrections, was performed in Ref. [185]. (Note, however, that the use of the expressions in [184] together with VFNS distributions, as implemented in the NuTeV analysis [102], is strictly not consistent.)

Comparison of the ν and $\bar{\nu}$ events found a preferred fit for the $s(x) - \bar{s}(x)$ distribution that peaked at $x \sim 0.05 - 0.1$, with the compensating negative contribution required by the sum rule $\int_0^1 dx (s - \bar{s}) = 0$ to be restricted to the unmeasured region at $x \lesssim 0.004$ [102]. For the first moment, the value obtained at $Q^2 = 16 \text{ GeV}^2$ was $S^- \equiv \int_0^1 dx x (s - \bar{s}) = (1.96 \pm 0.46 \pm 0.45 \begin{smallmatrix} +1.48 \\ -1.07 \end{smallmatrix}) \times 10^{-3}$, where the errors are statistical, systematic, and external. The latter includes a dominant contribution from the charm semileptonic branching ratio uncertainty, as well as from nuclear corrections [102].

The strangeness asymmetry in the nucleon is shown in Fig. 7 at $Q^2 = 16 \text{ GeV}^2$, as relevant for the NuTeV experiment, for several different PDF parametrizations. The MSTW08 [43] strange asymmetry is fitted to the CCFR and NuTeV data assuming the form

$$(s - \bar{s}) = a_0 x^{a_1} (1 - x)^{a_2} (1 - x/x_0), \quad (45)$$

where the factor $(1 - x/x_0)$ ensures zero net strangeness in the nucleon. The strange asymmetry in Ref. [177] is generated radiatively from the boundary condition

$(s + \bar{s})(x, Q_0^2) = 0$ at $Q_0^2 = 0.5 \text{ GeV}^2$, but allowing $s - \bar{s}$ to have the form in Eq. (45). The resulting $s - \bar{s}$ asymmetry at the experimental scale is similar to the MSTW08 fit, and to the phenomenological extraction in Ref. [102], within the currently sizable uncertainties.

The values for the momentum weighted asymmetry are the order $S^- \approx 2 \times 10^{-3}$ for the MSWT08 fit [43] and $S^- \approx 0.8 \times 10^{-3}$ for the dynamically generated PDFs [177] at scales $Q^2 \approx 10 - 20 \text{ GeV}^2$. The CTEQ Collaboration found a strange asymmetry in the range $-0.001 < S^- < 0.004$ [186]. These values have the correct sign and similar magnitude to that required to reconcile the NuTeV $\sin^2 \theta_W$ measurement with the Standard Model value [175], once the charge symmetry violating effects in Sec. 3.3 are also included [173].

Finally, a recent measurement by the ATLAS Collaboration [125] of inclusive W^\pm and Z boson production in pp collisions at the LHC found a significantly larger value of the strange to non-strange sea ratio in Eq. (44), $\kappa = 1.00_{-0.28}^{+0.25}$ at $x = 0.023$ for $Q^2 = 1.9 \text{ GeV}^2$, than in previous analyses. A reanalysis of the ATLAS and HERA data by the NNPDF group [49] found, however, that the uncertainty on the extracted κ was significantly underestimated, and that a more complete global analysis gives κ values consistent with the traditional values.

3.5. Heavy quarks

Heavy quark production contributes considerably to inclusive DIS; for example, the charm (bottom) contributions to the dominant F_2 structure function constitute up to 30% (3%) of the total in the small- x region. Besides these contributions, heavy quark electroproduction is directly accessed experimentally in semi-inclusive DIS, typically by detecting charm (bottom) mesons in the final state. Because the main production mechanism is photon-gluon fusion, data on this process provide valuable constraints on the gluon PDF in the nucleon. Furthermore, they provide an appropriate context for testing the different approaches to these calculations that have been adopted in various PDF analyses (see Sec. 2.4).

Since it is by far the most relevant, we focus the discussion on the charm flavor, although similar considerations often also apply to bottom (top contributions to this process, on the other hand, are negligible at accessible kinematics). The most relevant data on heavy quark electroproduction are the (H1 + ZEUS) combination of HERA measurements [15]. A comparison of these data with FFNS calculations at LO, NLO and NNLO* (see Sec. 2.4) in Fig. 8 (left) shows excellent agreement between the FFNS calculations. In fact, the experimental analysis of the HERA data is based primarily on the FFNS fully differential (exclusive) calculations of Ref. [188]. Despite this fact, the constructs in the GM-VFNSs are often motivated by arguing that pseudo-mass-divergences (non-collinear logarithms of the form $\ln Q^2/m^2$) which appear in the Wilson coefficients of the massive calculations need to be resummed. However, the FFNS results are notably stable even for very large values of $Q^2 \gg m^2$ [36], in particular at the largest

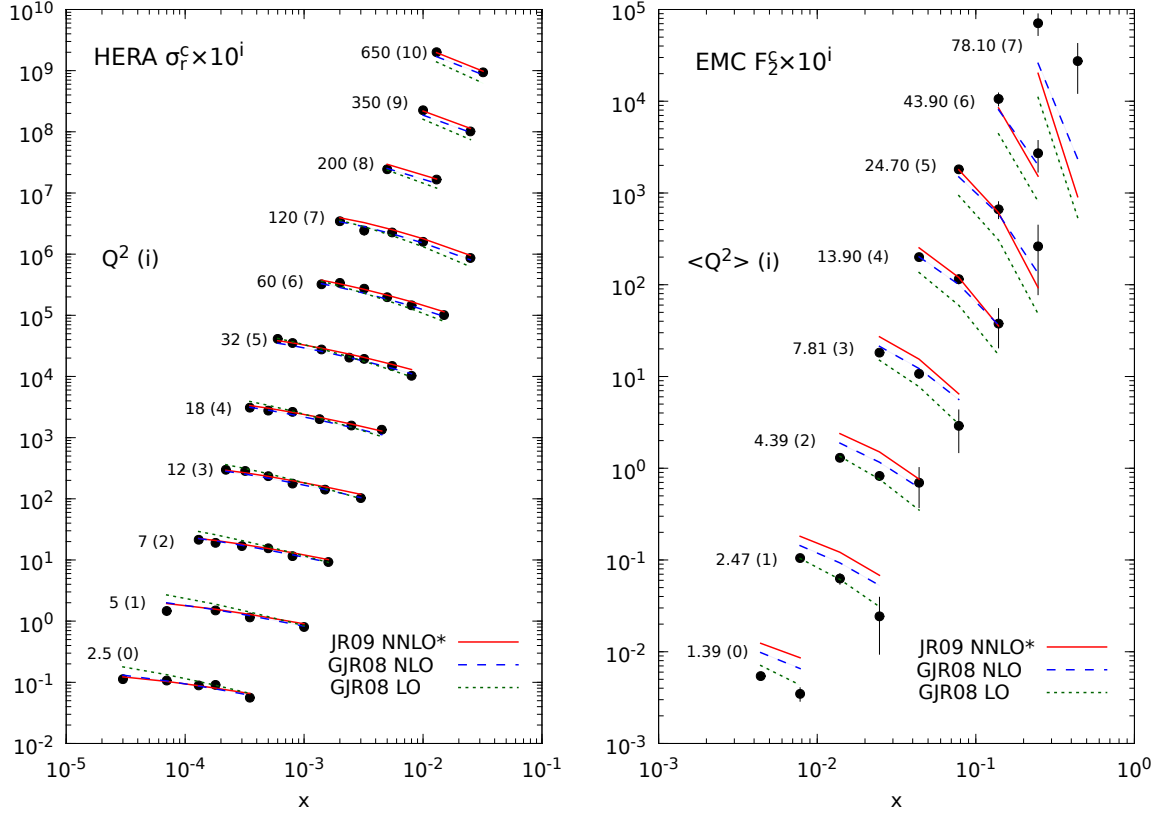


Figure 8. Reduced charm production cross section data from HERA [15] (*left*) and charm structure function data from EMC [194, 195] (*right*), compared with global PDF fits at LO, NLO and NNLO* [42, 41]. Note that for the EMC iron data the nuclear corrections of Ref. [187] were used.

Q^2 values accessible at HERA, suggesting little need to resum these supposedly “large logarithms” in the context of global PDF analyses.

Finally, in addition to the perturbative generation of charm, it is also possible for charm to be produced through nonperturbative mechanisms, such as those discussed in Refs. [33, 189, 190, 191, 192, 193] (and references therein). First postulated to account for some early charm production data in hadronic reactions, these “intrinsic” charm contributions share several characteristic features, even though their details depend somewhat on the models. In particular, they are typically valence-like, with significantly harder x distributions than those generated perturbatively, and can produce large asymmetries between the c and \bar{c} distributions.

Measurements of the charm structure function F_2^c by EMC [194, 195], especially the two data points at the highest Q^2 in Fig. 8 (right), have been interpreted as indicating a nonzero intrinsic charm contribution at large x . The evidence is not conclusive, however, in view of the disagreement evident in Fig. 8 (right) between the EMC data and theoretical predictions at smaller x , where the predictions are in agreement with the more recent HERA results in Fig. 8 (left).

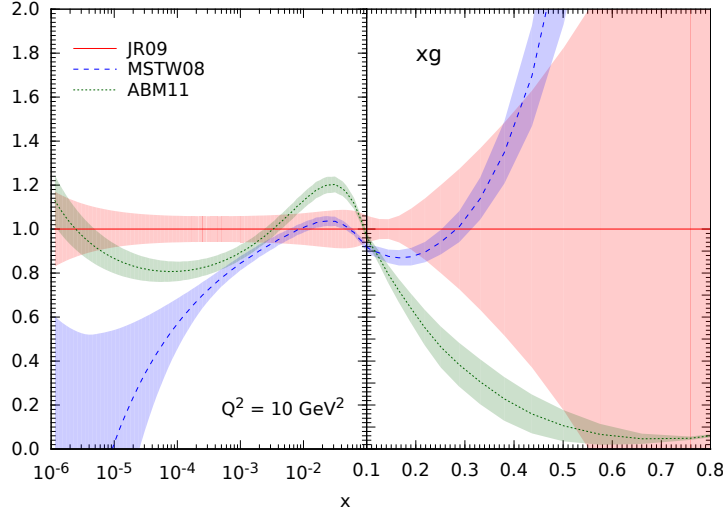


Figure 9. Gluon distributions for the 3-flavor NNLO PDF sets from JR09 [42] (red solid line), MSTW08 [43] (blue dashed) and ABM11 [40] (green dotted), relative to the JR09 gluon PDF, at $Q^2 = 10 \text{ GeV}^2$.

The current limits on the normalization of the nonperturbative charm quark distribution range from $\sim 0.5\%$ to 2% , depending on which data sets are fitted and which models of intrinsic charm considered [33, 43, 189, 192, 193, 196, 197]. Although current global PDF analyses do not require an intrinsic charm component, the existence of nonperturbative charm remains an intriguing issue which can be addressed by high-precision measurements of charm production at future facilities such as J-PARC [168, 198], GSI-FAIR [199], Jefferson Lab at 12 GeV [200, 201], AFTER@CERN [202], or an Electron-Ion Collider [113].

3.6. Gluons

In addition to the heavy quark production discussed above, there are three primary sources of information on the gluon distribution: the Q^2 dependence of the DIS structure function F_2 at low values of x ; the longitudinal structure function F_L at all x values; and jet (both at HERA and at hadron colliders) and photon production cross sections at moderate to high values of x . Furthermore, the momentum sum rule (32) provides an additional constraint on the gluon PDF. Since the normalizations of the valence PDFs are fixed by the flavor sum rules in Eq. (31) and the contributions of the light antiquarks are relatively well determined by DIS and lepton pair production data, the momentum sum rule effectively constrains the gluon contribution. The effect is an anticorrelation between the low- and high- x behavior of the gluon PDF: a decrease (increase) of the gluon distribution at low x leads to an increase (decrease) at high values of x . Interestingly, this can result in more constrained gluon distributions in the medium- x region (see Fig. 9).

To understand the relationship between the scale dependence of F_2 and the gluon

PDF, consider Eq. (8) for the scale dependence of the quark PDF. Multiply both sides by x and by the squared parton charge and sum over the active flavors. In this way one derives (using the LO expression for F_2),

$$Q^2 \frac{\partial F_2(x, Q^2)}{\partial Q^2} = \int_x^1 dy \left[P_{qq}(y, Q^2) F_2\left(\frac{x}{y}, Q^2\right) + \sum_i e_i^2 P_{qg}(y, Q^2) \frac{x}{y} g\left(\frac{x}{y}, Q^2\right) \right] \quad (46)$$

where P_{qq} and P_{qg} are the quark–quark and quark–gluon splitting functions. At small values of x the gluon term dominates the integrand so that the scale dependence of F_2 places a constraint on the gluon PDF.

A second constraint on the gluon from DIS comes from the longitudinal structure function F_L , which is defined as

$$F_L(x, Q^2) = \left(1 + \frac{4M^2 x^2}{Q^2}\right) F_2(x, Q^2) - 2xF_1(x, Q^2) \xrightarrow{Q^2 \rightarrow \infty} F_2(x, Q^2) - 2xF_1(x, Q^2). \quad (47)$$

In lowest order, where only quarks contribute to F_1 and F_2 , one has $F_2 = 2xF_1$ so that $F_L = 0$. The first nonzero contribution to F_L starts at $\mathcal{O}(\alpha_s)$ where, at small x , there is a significant contribution from the subprocess $\gamma^* g \rightarrow q\bar{q}$, which again imposes strong constraints on the gluon PDF at small x . At larger x values the valence quark contributions increase, the gluon PDF decreases, and the subprocess $\gamma^* q \rightarrow qg$ dominates. However, since the same combinations of quark distributions are well determined from F_2 , where they enter with one power of α_s less and the gluon does not contribute, precision measurements of the longitudinal structure function provide valuable information on the gluon PDF at large x [203].

Note also that the gluon PDF is accompanied by the same powers of α_s in all DIS structure functions, starting with $\alpha_s g$. This results in a correlation between the value of α_s obtained in global PDF analysis and the size and shape of the gluon distribution, with larger α_s leading to a smaller gluon PDF in the small- x region and (via the momentum sum rule correlation) a larger gluon PDF at large x . This can be seen in Fig. 9, where the JR09 [42] and ABM11 [40] analyses obtain α_s values and small- x gluon PDFs of similar size, while the MSTW08 fit [43] finds a larger α_s value and a smaller gluon PDF in this region (which even turns negative). Both possibilities describe well the inclusive cross sections measurements at HERA.

This ambiguity can be reduced by using processes with a different leading α_s power, typically jet production at the Tevatron, which, as noted in Sec. 2.9.1, can provide constraints on the gluon PDF. To understand this, recall that the calculation of the jet cross section involves a sum over qq , qg and gg induced subprocesses where “ q ” stands for any flavor of quark or antiquark. At low values of jet x_T , the gg subprocesses dominate, at intermediate values all three contribute, and eventually as x_T approaches one only the qq terms survive – see Fig. 3 in Ref. [121], for example. Jet data at the Tevatron extend to x_T values of approximately 0.5, so these data provide some constraints on the gluon PDF, at least in the mid- x range where the qg subprocesses make substantial contributions.

As discussed in Ref. [129], isolated photon production at collider energies has the potential to tighten the error bands in the x range below about 0.2. It remains a challenge to find processes that will constrain the gluon beyond $x \approx 0.5$. The fundamental problem is that the valence PDFs here are larger than the gluon PDF. Most hard processes that receive contributions from qg subprocesses also receive contributions from qq processes, which reduce the sensitivity to the gluon PDF. One counterexample is provided by direct photon production in pp collisions. The two dominant subprocesses are initiated by $q\bar{q}$ and qg initial states. At large values of x_T the fragmentation process is suppressed; it can be further reduced by photon isolation cuts. The single photon cross section involves an integration over the awayside jet rapidity which tends to smear out the x values of the contributing PDFs. There are regions where one x is small and one is large — one might think that this could constrain the large- x gluon. However, the favored configuration will be where the gluon or \bar{q} is at small values of x while the valence quark is at the larger values. Instead, consider the photon + jet cross section with equal and opposite photon and jet rapidities, in which case both momentum fractions will be equal to $x_T \cosh y_\gamma$ using LO kinematics. Going to large values of x_T and $y_\gamma = -y_{jet}$ would then yield information on the gluon at large x , since the \bar{q} contribution is much smaller there than that of the gluon. This would also be the case for lepton pair [204] and vector boson production in pp collisions, provided that one considers $p_T \gtrsim M_B/2$ in order for the parton momentum fraction to be large. The analysis in Ref. [205] suggests that photon + jet data with increased statistics from the LHC may help constrain the gluon and light quark PDFs.

Another source of information on the gluon PDF is top quark pair production, for which the lowest order subprocess is $gg \rightarrow t\bar{t}$. In Ref. [206] the constraints on the gluon PDF provided by $t\bar{t}$ data from the Tevatron and LHC were examined, with the results indicating that these data place strong constraints on the large- x gluon PDF. Also of note is the analysis of ratios and double ratios of cross sections measured at different LHC energies [207]. Such ratios have reduced systematic errors and have the potential to provide strong constraints on large- x PDFs.

In addition to the issues discussed above, an obstacle for the determination of the gluon distribution, and the highly correlated α_s values from PDF analysis, is that the calculations for the relevant processes are not available beyond NLO, with the important exceptions of the (light quark contributions to the) inclusive DIS structure functions and Drell-Yan cross sections. For example, the relative uncertainties of the JR09 gluon PDF in Fig. 9 are below about 10% for $x \lesssim 0.1$, and increase as one proceeds to higher values of x , where the constraints of the F_2 structure function from fixed target experiments used in that fit are weaker. The uncertainty at large x could in principle be reduced by including jet data. However, this would also affect the central values obtained for the gluon PDF, changing them in the relevant region by an amount proportional to the missing NNLO corrections, which in the case of jet production are expected to be large [208]. Global NNLO fits which include jet data, such as the MSTW08 [43] parametrization in Fig. 9, generally find larger gluon PDFs in the high- x region and

correspondingly also larger values of α_s .

Yet another factor which can alter the PDFs and the value of α_s obtained in a particular analysis are the kinematic cuts applied; of particular relevance are the cuts on the DIS structure function data and the related treatment of contributions beyond leading twist [40, 122]. Although data selection (data sets and cuts) bring about certain arbitrariness in global PDF analysis, it cannot account for all the existing differences between the various PDF sets, which are also affected by theoretical issues such as heavy quark schemes (Sec. 2.4) and the particular solutions of the RGE equations used. Even within a given framework there are uncertainties due to the inability of the estimation procedure to find the optimal solution, for example, shortcomings of the parametrization to reproduce the optimal shape of the distributions, and the statistical estimation procedure. These effects, referred in general as ‘procedural bias’, induce a dependence of the results on the choice of the scale at which the input distributions are parametrized, which in principle should not depend on these choices. For particularly sensitive quantities such as the gluon distribution and α_s , this uncertainty can be comparable to the experimental uncertainty [122], as can be seen in Fig. 10.

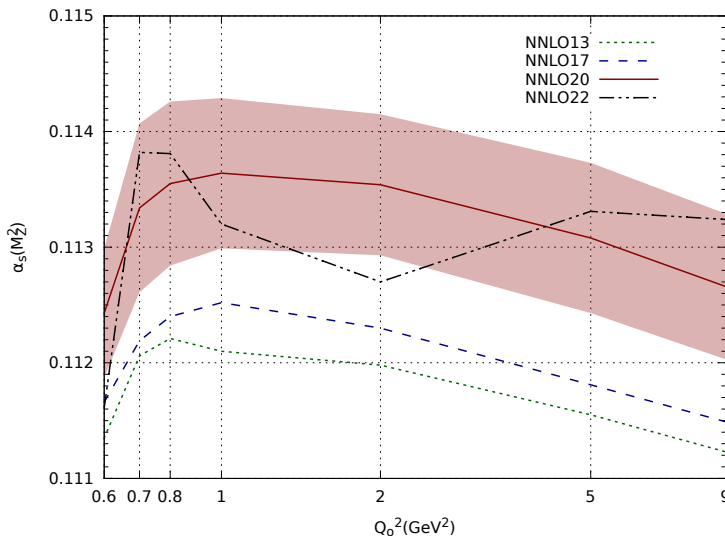


Figure 10. Input scale dependence of $\alpha_s(M_Z^2)$ values obtained for different parametrizations in Ref. [122]. The band indicates the uncertainties due to propagation of the experimental errors for a particular parametrization (NNLO20).

Another example of this is the differences between “standard” distributions, generated from input PDFs at values for the input scale $Q_0^2 \geq 1 \text{ GeV}^2$, and the so-called dynamical distributions [37, 38, 41, 209], for which input scale is chosen to be $Q_0^2 < 1 \text{ GeV}^2$. At these low scales the input distributions naturally tend to valence-like (positive definite) shapes [122] that vanish in the small- x limit, not only for valence but also for the sea quark and gluon input densities. It was shown in Refs. [41, 209], where also “standard” distributions were generated, that this implies that the dynamical

distributions at small x are more restricted and have smaller uncertainties than their standard counterparts. Furthermore, this procedure typically results in smaller α_s values and steeper gluons in the small- x region, although both approaches provide comparable descriptions of data, in particular, of the inclusive DIS cross sections from HERA.

An alternative approach to fitting α_s as part of the global fitting is to use the world average value for $\alpha_s(M_Z)$, thereby avoiding the correlations during the fitting process. Since α_s is a parameter of the QCD Lagrangian, it should be the same for all processes, not just those in the global fit. Of course, interesting information could be obtained by determining the PDFs both with a fixed value of $\alpha_s(M_Z)$ and with a fitted value. Comparing the results could indicate which processes in the global fit are chiefly responsible for any differences.

3.7. Lattice PDF moments

The moments of leading twist PDFs can be evaluated from first principles using lattice QCD. Within the operator product expansion, the moments of PDFs are related to matrix elements of local operators between hadron states, which can be computed numerically on the lattice. The lattice PDF moments can be related to the quark and antiquark distributions in the nucleon as

$$\langle x^n \rangle_q = \int_0^1 dx x^n [q(x) - (-1)^n \bar{q}(x)], \quad (48)$$

$$\langle x^n \rangle_{\Delta q} = \int_0^1 dx x^n [\Delta q(x) + (-1)^n \Delta \bar{q}(x)], \quad (49)$$

for the unpolarized and helicity distributions (see Sec. 4), respectively. The lattice moments alternate between the total (or C -even) $q + \bar{q}$ and valence (C -odd) $q - \bar{q}$ distributions, depending on whether n is even or odd. While reconstructing the x dependence of the PDFs from a finite number of calculated moments is challenging [210], comparison of the lattice moments with the phenomenological PDF moments can provide important tests of lattice techniques and provide constraints on specific PDFs which may be difficult to measure experimentally.

Because of the discretization of space-time on the lattice, the rotational symmetry of the continuum is broken to the hyper-cubic subgroup, which introduces mixing with lower dimensional operators under renormalization. As a result, only the lowest few moments, corresponding to $n \leq 3$, can at present be reliably computed. As well as the usual approximations of working at a finite lattice spacing a , in a finite lattice volume V , and at unphysically large values of the quark mass, simulations usually include contributions only from “connected” diagrams, representing operator insertions on quark lines connected to the source. Meaningful comparisons of lattice data can therefore only be made with nonsinglet combinations, such as $u - d$, where the “disconnected” contributions cancel.

Significant progress has been made in recent years in the computation of matrix elements of twist-two operators on the lattice, using dynamical (unquenched)

configurations and quark (or pion, by the Gell-Mann–Oaks–Renner relation) masses approaching the physical limit. Unfortunately, the results for the lowest nontrivial ($n = 1$) nonsinglet moment of the unpolarized distributions, $\langle x \rangle_{u-d}$, lie systematically in the range $\approx 0.23 - 0.25$ at a scale $\mu^2 = 4 \text{ GeV}^2$, which is some 40% above the phenomenological PDF moments of $\langle x \rangle_{u-d} \approx 0.17$ [2]. A smaller, but persistent 10% overestimate of the lowest ($n = 0$) moment of the nonsinglet spin-dependent distribution, $\langle 1 \rangle_{\Delta q} = g_A$, has posed a serious challenge to lattice simulations [211, 212].

It has been suggested [213, 214, 215] that the discrepancy between the calculated and experimental PDF moments could be resolved by the nontrivial chiral behavior of the moments, when extrapolating the results from the lowest m_π values at which lattice data exist to the physical mass. Verification of this behavior will require lattice simulations at very small quark masses, as well as at large enough volumes to fully include the physics of the pion cloud [216] (see also Sec. 3.2). While it may take some time before the lattice parameters can become sufficiently close to those in the physical realm, such comparisons will continue to reflect the important synergy between lattice QCD and PDF phenomenology.

4. Spin-dependent parton distributions

Considerable progress has been made in understanding the spin structure of the nucleon since the first precision polarized DIS experiments at CERN in the late 1980s [217] indicated an anomalously small fraction of the proton spin carried by quarks. A rich program of spin-dependent inclusive and semi-inclusive DIS, as well as polarized proton–proton scattering experiments has followed, vastly improving our knowledge of spin-dependent PDFs of the nucleon over the last two decades (for a recent review, see Ref. [8] and references therein).

While the spin-dependent data have not been as abundant as those available for constraining spin-averaged PDFs, the existing empirical information from polarized lepton and hadron facilities at CERN [217, 218, 219, 220, 221, 222], SLAC [223, 224, 225, 226, 227, 228], DESY [229, 230, 231, 232, 233], Jefferson Lab [234, 235, 236, 237, 238] and RHIC [239, 240, 241, 242, 243, 244] has enabled several dedicated global QCD analyses of spin-dependent parton distributions to be performed. These include the NLO analyses from the more established DSSV [245] group, the European-based LSS [75] and BB [76] groups, as well as the Japanese Asymmetry Analysis Collaboration (AAC) [246], using the standard global fitting methodology outlined in Sec. 2. More recent efforts have been made by the NNPDF Collaboration [247], extending the neural network approach to the polarized sector, and the Jefferson Lab Angular Momentum (JAM) Collaboration [79], which has focused on utilizing data over a large kinematic range that includes the large- x and low- Q^2 regions, with a simultaneous fit of unpolarized PDFs.

Representative examples of the spin-dependent PDFs are shown in Fig. 11, illustrating the total (or C -even) Δu^+ and Δd^+ PDFs, as well as the sea quark $\Delta \bar{u}$, $\Delta \bar{d}$ and $\Delta \bar{s}$ and polarized gluon Δg distributions, for the DSSV09 [245], LSS10 [75],

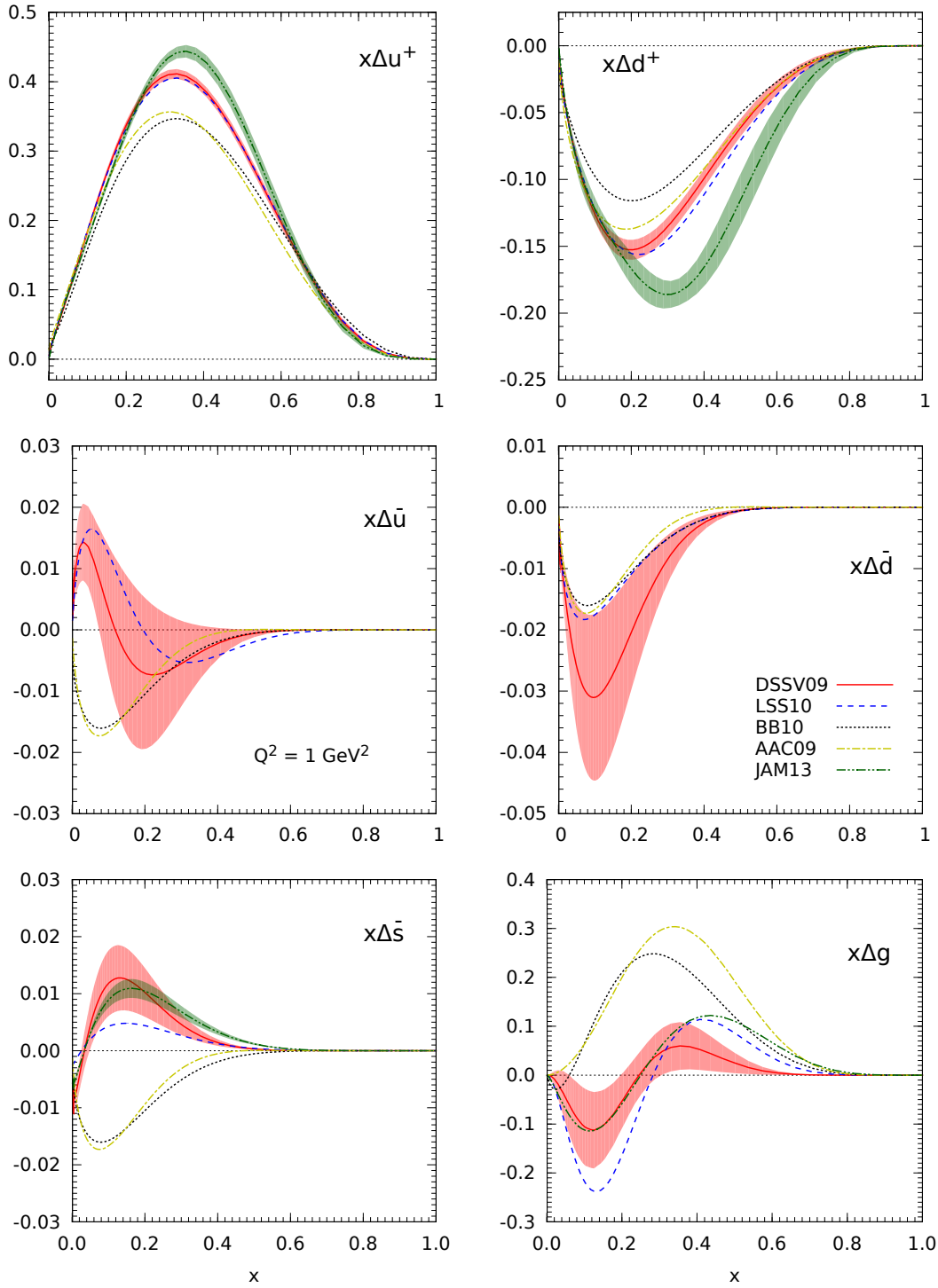


Figure 11. Comparison of the spin-dependent PDFs for the total $x\Delta u^+ = x(\Delta u + \Delta \bar{u})$ and $x\Delta d^+ = x(\Delta d + \Delta \bar{d})$, the antiquark $x\Delta \bar{u}$, $x\Delta \bar{d}$ and $x\Delta \bar{s}$, and polarized gluon $x\Delta g$ distributions at $Q^2 = 1 \text{ GeV}^2$, for the DSSV09 [245], LSS10 [75], BB10 [76], AAC09 [246], and JAM13 [79] PDF sets.

BB10 [76], AAC09 [246], and JAM13 [79] PDF sets at $Q^2 = 1 \text{ GeV}^2$. The BB10 [76] and JAM13 [79] analyses are based on inclusive DIS data only, while the LSS10 [75] fit includes also semi-inclusive DIS data. The DSSV09 PDFs are constrained in addition by polarized pp scattering data. The latest AAC analysis [246] is based on inclusive DIS data and a K -factor approximation for the NLO corrections for the pp data.

As for the unpolarized case in Fig. 2, the Δu^+ distribution is the best constrained polarized PDF, mostly by measurements of the proton g_1 structure function over a relatively broad range of x . The corresponding Δd^+ distribution, which has the opposite sign, is smaller in magnitude compared with the Δu^+ with somewhat larger uncertainties, especially at larger x values. The uncertainty band for the DSSV09 parametrization of Δu^+ and Δd^+ is smaller than the variation between the different PDF sets, which reflects the fact that the systematic uncertainties associated with the choice of data sets and parametrization assumptions, as well as other theoretical inputs, are currently larger than the experimental errors.

The polarization of the sea is considerably smaller, and more strongly dependent upon assumptions about the flavor dependence in the analysis of semi-inclusive DIS data. At present there is no conclusive experimental evidence of a nonzero light quark sea, $\Delta \bar{u}$ and $\Delta \bar{d}$, although there is a slight trend towards a more negatively polarized \bar{d} distribution than \bar{u} , with a positive $\Delta \bar{u} - \Delta \bar{d}$. The polarization of the strange sea is also very small, in contrast to suggestions from the early spin-dependent DIS data analyses of a large negative $\Delta \bar{s}$. The polarized gluon distribution is essentially unconstrained by existing inclusive and semi-inclusive DIS data, and almost all information on Δg comes from measurements of $c\bar{c}$ production in semi-inclusive DIS [248], and inclusive pion and jet production in polarized pp scattering [239, 240, 241, 243, 244]. The data are consistent with a small value of $\Delta g/g$, consistent with zero, although new measurements from RHIC have the promise of resolving a small nonzero distribution.

4.1. Polarized valence quarks at large x

At large values of x , the spin-dependent PDFs are even more sensitive to the quark-gluon dynamics responsible for spin-flavor symmetry breaking than the spin-averaged valence quark PDFs discussed in Sec. 3.1. However, while considerable progress has been made in determining spin-dependent PDFs over the last two decades, especially in the small- x region, relatively little attention has been paid to structure function measurements at large x .

The dearth of data in the valence region is especially striking for the neutron, where, with the exception of several data points from Jefferson Lab Hall A [234] for the polarization asymmetry A_1^n extending to $x \approx 0.6$, there are essentially no constraints for $x \gtrsim 0.4$. On the other hand, there are a number of predictions for the behavior of polarized PDFs and ratios of polarized to unpolarized PDFs in the limit as $x \rightarrow 1$ that differ even in sign.

At large x there are dramatically different predictions for the valence Δu and

Δd distributions from nonperturbative and perturbative calculations. In the simple SU(6) spin-flavor symmetric quark model, the equal probabilities of the spin-0 and spin-1 spectator diquark configurations lead to the simple relation $\Delta d/\Delta u = -4$, and corresponding polarized to unpolarized ratios $\Delta u/u = 2/3$ and $\Delta d/d = -1/3$. In this limit the polarization asymmetry of the proton, which at LO can be written

$$A_1^p \approx \frac{4\Delta u^+ + \Delta d^+}{4u^+ + d^+}, \quad (50)$$

is predicted to be $A_1^p = 5/9$, while that of the neutron,

$$A_1^n \approx \frac{\Delta u^+ + 4\Delta d^+}{u^+ + 4d^+}, \quad (51)$$

would vanish, $A_1^n = 0$.

While spin-flavor symmetry is of course broken in nature (in some cases badly), with the unpolarized d quark distribution significantly softer than the u , for example, the details of this breaking can affect the spin-dependent PDFs in strikingly different ways. The mechanism of spin-1 diquark suppression, which leads to the vanishing of the d/u ratio as $x \rightarrow 1$, also predicts that $\Delta u/u \rightarrow 1$ in this limit, while $\Delta d/d$ remains unchanged from the SU(6) expectation.

Arguments based on helicity conservation in perturbative QCD, on the other hand, predict that for valence quarks in the ground state of the nucleon the scattering at large x is predominantly from configurations in which the quark is coupled to a diquark of zero helicity [136]. In this case the PDFs associated with a quark polarized in the same direction as the nucleon are favored over the helicity-antialigned configurations, $q^\uparrow(x) \gg q^\downarrow(x)$ as $x \rightarrow 1$. This model leads to the expectation that $\Delta u/u \rightarrow 1$ and $\Delta d/d \rightarrow 1$ in the $x \rightarrow 1$ limit, and consequently a rapid approach to unity of both the proton and neutron A_1 asymmetries.

An additional feature of the helicity conservation model is that it correlates the $x \rightarrow 1$ behavior of the PDFs with the large- Q^2 behavior of elastic form factors [137, 138, 139], which can be measured in elastic lepton–nucleon scattering experiments at Jefferson Lab and elsewhere [249]. This is also closely related to the notion of quark-hadron duality, which connects averages over structure functions in the resonance region at low W with those extrapolated from the deep-inelastic continuum at higher W (lower x) [48, 250, 251]. Since the existing DIS data are for the most part consistent with a vanishingly small neutron asymmetry at $x \lesssim 0.5$, a very dramatic change in A_1^n would be expected at larger x . An even more rapid transition at high x may occur if quark orbital angular momentum plays an important role in nucleon structure [252].

Experimentally, the extraction of leading twist spin-dependent PDFs at high x faces similar challenges to those discussed in Sec. 3.1 for the unpolarized distributions. In particular, information on the structure of the neutron is typically obtained from experiments involving polarized deuterium or ^3He nuclei, requiring the nuclear corrections to be understood. Analysis of high- x data also necessitates careful treatment of finite- Q^2 corrections such as target mass and higher twist contributions. The effects of these corrections are illustrated in Fig. 12, which shows the total Δu^+ and Δd^+ PDFs

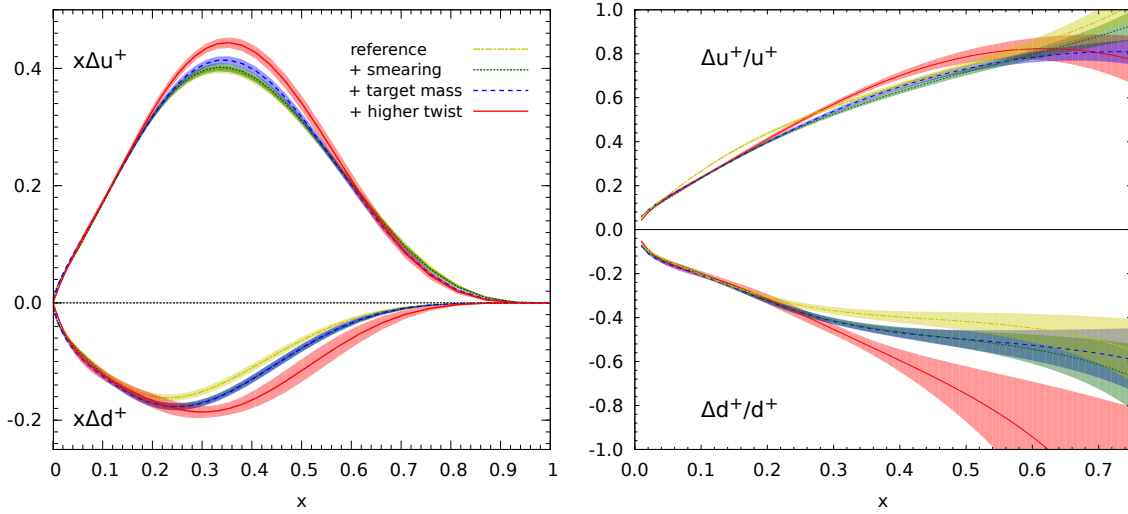


Figure 12. (Left) Polarized $x\Delta u^+$ and $x\Delta d^+$ distributions and their uncertainties for the JAM13 PDF set [79] at $Q^2 = 1 \text{ GeV}^2$, illustrating the effects of the nuclear smearing (green dotted), target mass (blue dashed) and higher twist (red solid) corrections, relative to the reference fit (yellow dot-dashed). Note that the yellow and green bands overlap for $x\Delta u^+$ and the green and blue bands overlap for $x\Delta d^+$. (Right) Corresponding ratios of polarized to unpolarized $\Delta u^+/u^+$ and $\Delta d^+/d^+$ distributions.

from the JAM13 analysis [79] for various fits with or without the finite- Q^2 and nuclear corrections. At small values of x their effects are negligible; however, at $x \gtrsim 0.3$ they can give up $\sim 20\%$ corrections for Δu^+ and more $\sim 50\%$ corrections for Δd^+ (the relative correction can be even larger at $x \gtrsim 0.8$, although the PDFs are not constrained in this region).

The same effects are more clearly illustrated through the polarization ratios $\Delta u^+/u^+$ and $\Delta d^+/d^+$ in Fig. 12, where the unpolarized distributions are fitted simultaneously within the same analysis as the polarized [79]. This in principle eliminates any bias arising from the use of spin-averaged PDFs taken from analyses performed under different sets of assumptions. In the intermediate- x region the ratios for both u and d quarks are generally consistent with the symmetric quark model expectations, with the $\Delta u^+/u^+$ increasing towards unity at larger x . The $\Delta d^+/d^+$ ratio, on the other hand, remains negative for all x where it is constrained, and shows no indication of the upturn predicted by the helicity conservation models. The nuclear and finite- Q^2 effects can significantly impact the limiting behavior as $x \rightarrow 1$, and clearly additional data are needed in order to constrain their x dependence at high x . A dedicated program of large- x structure function measurements is planned at the 12 GeV energy upgraded Jefferson Lab facility [110, 111, 112]. More complete information on spin-dependent PDFs will also be available once the g_2 structure function of the nucleon is measured more accurately [253]. This will provide additional information on possible higher twist corrections that enter in the extraction of leading twist PDFs from DIS polarization asymmetries.

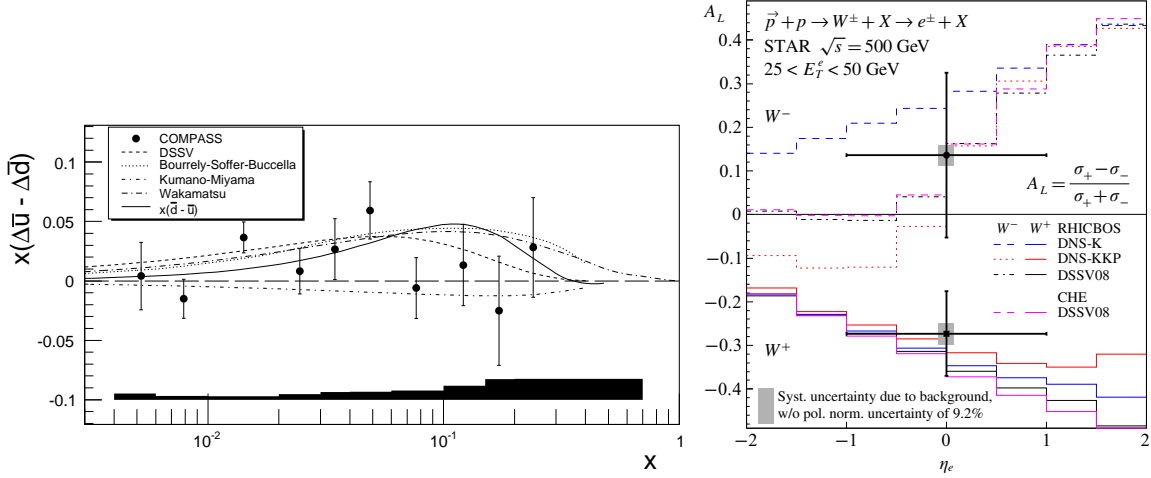


Figure 13. (Left) Flavor asymmetry of the polarized sea, $x(\Delta\bar{u} - \Delta\bar{d})$, from the COMPASS semi-inclusive DIS measurement at $Q^2 = 3 \text{ GeV}^2$ [222], compared with several parametrizations and model calculations, and the unpolarized $x(\bar{d} - \bar{u})$ asymmetry (solid curve). (Figure from Ref. [222].) (Right) Single polarization asymmetry A_L for inclusive W^\pm production in $\bar{p}p$ scattering from the STAR experiment at RHIC, at central electron pseudorapidity $\eta_e = 0$. (Figure from Ref. [242]. Copyright (2011) by the American Physical Society.)

4.2. Polarized sea quarks

As for the unpolarized inclusive charged lepton DIS measurements, inclusive g_1 structure function experiments measure C -even combinations of PDFs, Δq^+ . The individual quark and antiquark distributions can be separated with the help of semi-inclusive charged lepton scattering data, with coincident measurement of fast pions or kaons in the final state. Typically such experiments measure the semi-inclusive polarization asymmetry, which at LO can be written

$$A_1^h(x, z, Q^2) = \frac{\sum_q e_q^2 \Delta q(x, Q^2) D_q^h(z, Q^2)}{\sum_q e_q^2 q(x, Q^2) D_q^h(z, Q^2)}, \quad (52)$$

where $D_q^h(z, Q^2)$ is the fragmentation function for the scattered quark or antiquark to produce a hadron h ($h = \pi, K$) in the current fragmentation region with a fraction $z = E_h/\nu$. For large z , the produced hadron has a high probability of containing the scattered parton, hence providing a tag on the initial state distribution of quarks and antiquarks. The fragmentation functions D_q^h are extracted from independent fits to single hadron production cross sections in e^+e^- , pp and other reactions.

The program of semi-inclusive DIS measurements from proton and deuteron targets at HERMES [232], COMPASS [222], and earlier SMC [221], have produced intriguing glimpses into the flavor content of the polarized sea. The extracted sea quark and antiquark asymmetries are generally rather small, and consistent with zero within the current uncertainties. For the light quark polarized sea, there is a slight trend towards a positive $\Delta\bar{u}$ (with an x -integrated value of $+0.02 \pm 0.02$ (stat.) ± 0.01 (syst.)) from

the latest COMPASS data [222]) and a negative $\Delta\bar{d}$ (with an x -integrated value of -0.05 ± 0.03 (stat.) ± 0.02 (syst.)), so that the difference $\Delta\bar{u} - \Delta\bar{d}$ is slightly positive, at the 1.5σ level [222], as Fig. 13 indicates. This is in contrast to the large negative values of the unpolarized $\bar{u} - \bar{d}$ asymmetry (see Sec. 3.2), which would disfavor models such as the chiral quark soliton model in the large- N_c limit [254, 255] that predict large $\Delta\bar{u} - \Delta\bar{d} \gg \bar{d} - \bar{u}$. Very small antiquark spin asymmetries would be expected in models based on the pion cloud of the nucleon, such as those discussed in Sec. 3.2. One should caution, however, that the experimental distributions in Fig. 13 were extracted assuming LO expressions for the semi-inclusive asymmetries, which, strictly speaking, cannot be directly compared with NLO PDFs [245]. The comparison should therefore be viewed as a qualitative one, although the general indication of a small polarized non-strange sea is unlikely to be qualitatively modified in an NLO treatment.

The semi-inclusive DIS measurements are also consistent with a very small strange quark polarization, Δs . The HERMES data [233] give a slightly positive value when integrated between $x = 0.02$ and 0.6 , while the COMPASS data [222] are consistent with zero. This is in contrast with the analysis of inclusive DIS data on protons, deuteron and ^3He , which suggests a small negative value. The extractions of Δs from the inclusive and semi-inclusive data are somewhat dependent on the assumptions of SU(3) flavor symmetry for the axial charges of hyperons, and on the specific fragmentation functions used in the semi-inclusive analysis. Future measurements of kaon fragmentation functions D_q^K should improve the accuracy of the flavor decomposition of the proton's helicity distributions.

A complementary method, discussed by Bourrely and Soffer [256], of constraining the $\Delta\bar{u}$ and $\Delta\bar{d}$ distributions, which does not depend on knowledge of fragmentation functions, is through longitudinal polarization asymmetries in inclusive W^\pm boson production from pp scattering with one proton polarized and the other unpolarized, $\vec{p}p \rightarrow W^\pm X \rightarrow e^\pm X$. The asymmetry for W^- production, for example, can then be written at LO as [257]

$$A_L^{W^-} = \frac{\Delta\bar{u}(x_a) d(x_b)(1 - \cos\theta)^2 - \Delta d(x_a) \bar{u}(x_b)(1 + \cos\theta)^2}{\bar{u}(x_a) d(x_b)(1 - \cos\theta)^2 + d(x_a) \bar{u}(x_b)(1 + \cos\theta)^2}, \quad (53)$$

where θ is the scattering angle of the electron in the partonic center-of-mass frame, while the corresponding W^+ asymmetry at LO is

$$A_L^{W^+} = \frac{\Delta\bar{d}(x_a) u(x_b)(1 + \cos\theta)^2 - \Delta u(x_a) \bar{d}(x_b)(1 - \cos\theta)^2}{\bar{d}(x_a) u(x_b)(1 + \cos\theta)^2 + u(x_a) \bar{d}(x_b)(1 - \cos\theta)^2}. \quad (54)$$

At large negative rapidity, where $x_a \ll x_b$, the W^- asymmetry then directly probes the $\Delta\bar{u}$ PDF, $A_L^{W^-} \sim \Delta\bar{u}(x_a)/\bar{u}(x_a)$, while at large positive rapidity one has $x_a \gg x_b$, and the asymmetry is sensitive to the Δd PDF at large x , $A_L^{W^-} \sim -\Delta d(x_a)/d(x_a)$. For W^+ production, the term proportional to $\Delta\bar{d}(x_a)$ will be similarly enhanced at small $x_a \ll x_b$; however, the angular factor will produce a suppression of this contribution at backward angles relative to the $\Delta u(x_a)$ term, so that both terms will give competing contributions.

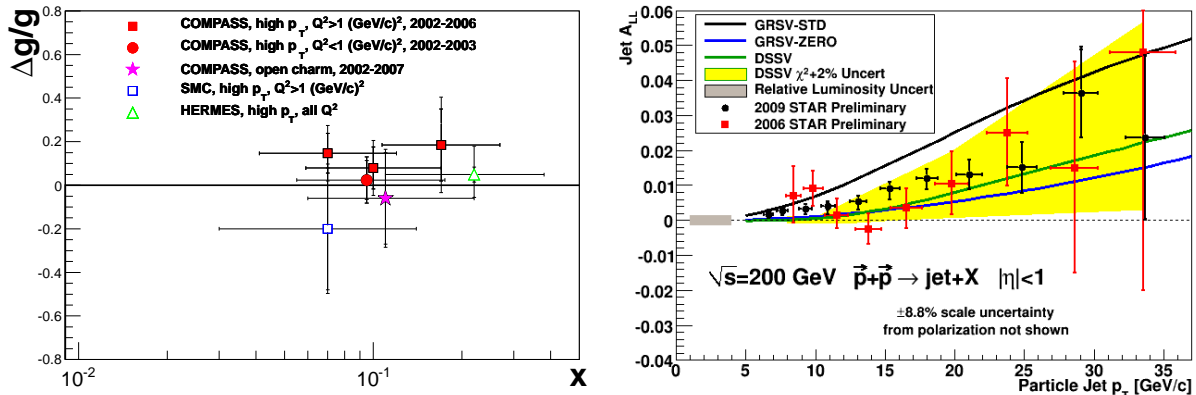


Figure 14. (Left) Gluon polarization ratio $\Delta g/g$ values extracted at LO from charm and high- p_T hadron production data from COMPASS, SMC and HERMES. (Figure from Ref. [248]. Copyright (2013) by the American Physical Society.) (Right) Longitudinal double-spin asymmetry A_{LL} for inclusive jet production, as a function of the jet transverse momentum, in polarized $\vec{p}\vec{p}$ scattering from the STAR experiment at RHIC [243], compared with calculations based on several PDF parametrizations. (Figure from Ref. [244].)

The first data from the STAR experiment (Run 9) at RHIC [242] are shown in Fig. 13 for zero electron rapidity, and are generally in agreement with NLO calculations using existing PDF parametrizations. Data from Run 12 at RHIC have subsequently been taken at both forward and backward rapidities [258], and will provide important constraints on the antiquark polarization.

4.3. Gluon helicity

Information on the polarized gluon distribution Δg can be obtained in several complementary ways. Firstly, from the Q^2 evolution equations, the evolution of the quark singlet contribution to the g_1 structure function mixes with the gluon contribution, so that in principle the study of scaling violations in g_1 can constrain Δg . In practice, however, the Q^2 range and precision of the available inclusive DIS data are not sufficient to provide meaningful constraints, and DIS-only fits of spin-dependent PDFs effectively leave Δg undetermined.

More direct information on gluon polarization has come from the production of charm mesons and high- p_T hadrons in semi-inclusive DIS, through the process of photon-gluon fusion (see Sec. 3.5). Data on hadron production from HERMES, SMC and COMPASS, and open charm data from COMPASS have been analyzed over a range of x values, averaging from $\langle x \rangle = 0.07$ to ≈ 0.2 , and Q^2 between $\approx 1 \text{ GeV}^2$ and 13 GeV^2 . Most of the analyses have been performed at LO, finding values of $\Delta g/g$ consistent with zero, albeit with large uncertainties, as illustrated in Fig. 14. The recent COMPASS experiment [248] was the first to be analyzed at NLO, yielding

$\Delta g/g = -0.13 \pm 0.15$ (stat.) ± 0.15 (syst.) over the range $0.12 < x < 0.33$ with an average $\langle x \rangle \approx 0.2$.

An alternative reaction that can be used to constrain Δg is the inclusive production of jets or neutral pions in polarized proton–proton scattering. The longitudinal double-spin asymmetry for this process,

$$A_{LL} = \frac{\sigma^{++} - \sigma^{+-}}{\sigma^{++} + \sigma^{+-}}, \quad (55)$$

where $\sigma^{++}(\sigma^{+-})$ is the differential cross section for longitudinally polarized protons with equal (opposite) helicities, is then sensitive to the polarized quark–gluon scattering cross section at the parton level. Following an early measurement of A_{LL} for multi- γ pairs from two-jet type events by the Fermilab E581/704 Collaboration [239], which found a small $\Delta g/g$ at $0.05 \lesssim x \lesssim 0.35$, most of the experimental effort at measuring Δg in pp scattering has been by the PHENIX and STAR Collaborations at RHIC.

The STAR experiment measures inclusive jet production in $\vec{p}\vec{p} \rightarrow \text{jet} + X$ at an invariant center of mass energy $\sqrt{s} = 200$ GeV. The A_{LL} data from the 2006 and 2009 runs [243, 244] shown in Fig. 14 provide the clearest evidence to date for a small but nonzero Δg . A nonzero asymmetry is also observed by STAR in preliminary data on dijet events at mid-rapidity [259], which may provide even better constraints on the shape of Δg .

The PHENIX data on inclusive neutral pion production, $\vec{p}\vec{p} \rightarrow \pi^0 + X$, from 2005 to 2009 suggest a very small asymmetry up to $p_T \approx 10$ GeV [240, 241]. Taken together, the inclusive RHIC data from several different channels suggest a small but non-vanishing gluon polarization in the proton. Though not as large as had been proposed in some early explanations of the small contribution of quarks to the proton spin, the precise role played by Δg in the proton spin budget will be intriguing to understand from future measurements.

5. Outlook

In this topical review we have presented a summary of the current knowledge of spin-averaged and (longitudinal) spin-dependent PDFs. While great progress has been made in recent years, there are still regions of Bjorken- x where the PDF uncertainty bands are uncomfortably large. This is primarily due to either lack of data in kinematic regions that would otherwise provide constraints on the PDFs, or to the particular PDF being smaller in that region than those of other flavors, or both. One might naively conclude that if existing data do not constrain particular PDFs in certain domains, then it may not be too important to seek ways to constrain them there. However, this viewpoint overlooks two important points: (i) there is intrinsic interest in the behavior of the different PDFs and relations to the properties of the parent hadrons, and (ii) it is possible that new phenomena may occur in extended kinematic regions which would require precise knowledge of the PDFs there.

As an example, suppose one were searching for a massive state produced at large rapidity in hadron-hadron collisions. This would typically require one parton to have a large value of x and the other a small value. The errors at large x may well dominate the uncertainty in the resulting prediction. The key here is to measure Standard Model processes in expanded kinematic regions and include these processes in the global fits. The resulting reduction in the errors can then be used to improve searches for new phenomena in these regions. Moreover, if one reduces the errors at large values of x , this will necessarily lead to reductions in the errors at intermediate x .

Since deuterium targets in DIS are a prime source of information on the d quark PDF at large values of x , nuclear corrections are a significant source of uncertainty in its determination. Several planned experiments at the 12 GeV energy upgraded Jefferson Lab [144, 143, 145] will use techniques that reduce the effects of nuclear corrections on the extraction of d/u at large x . Constraints on the d/u ratio in the proton can also be obtained, free of nuclear effects, through the measurement of W^\pm charge asymmetries in pp collisions at very high rapidity [100], although this would require reconstruction of the W^\pm distributions themselves from the decay lepton distributions and, unlike in $p\bar{p}$ collisions at the Tevatron, would require precise knowledge of the \bar{u} and \bar{d} distributions [124].

Another important area of investigation is the flavor separation of the PDFs. For example, currently our knowledge of the s and \bar{s} PDFs comes primarily from one neutrino experiment which used an iron target [102], thus requiring the use of model-dependent nuclear corrections. Other sources, for example weak vector boson production at the LHC [125], can provide additional constraints, especially as the statistics of the measurements improve. In a complementary effort, the HERMES Collaboration has measured [233] K^\pm production in semi-inclusive DIS and used these data to place constraints on the strange quark PDF. While an interesting analysis, it does depend on knowledge of the K^\pm fragmentation functions, and a recent, more complete analysis [260] of the HERMES data suggests a somewhat smaller s PDF than that extracted in Ref. [233]. Better knowledge of the fragmentation functions would clearly help in the interpretation of the semi-inclusive DIS measurements. Ideally, a high statistics neutrino experiment on *hydrogen* could further provide knowledge of both the s and \bar{s} PDFs through the measurement of charm production (using the $\nu s \rightarrow \mu^- c$ and $\bar{\nu} \bar{s} \rightarrow \mu^+ \bar{c}$ subprocesses) without having to make model-dependent nuclear corrections. Note that such an experiment could also yield information on the d/u ratio at high values of x .

Information on the SU(2) flavor asymmetry of the proton sea will be provided by Experiment E906/SeaQuest [166] at Fermilab, which is currently taking data on muon pair production using a 120 GeV proton beam on a variety of targets. It is designed to improve our knowledge of $\bar{d} - \bar{u}$ over the x range out to $x \sim 0.45$, whereas the currently available data run out of statistics at $x \approx 0.3$. The experiment will further enable a study of the effects of nuclear binding on the sea quark PDFs. There is also the possibility of follow-on measurements of lepton pair production at the Nuclear and Particle Physics facility at J-PARC [167, 168] in Japan.

The question of charge symmetry violation in PDFs can be addressed in future through study of Drell-Yan lepton pair production in π^\pm scattering from the deuteron, which could be measured at the Fermilab Main Injector or with the COMPASS experiment at CERN [172], or via measurement of π^+/π^- electroproduction ratios in semi-inclusive DIS from isoscalar targets [261]. Another avenue to explore will be parity-violating DIS on a deuterium target [262, 263], for which the parity-violating asymmetry arising from $\gamma - Z$ interference is expected to be independent of hadronic structure at large x in the absence of CSV effects [65, 264, 265, 266]. Beyond searches for CSV effects, a program of parity-violating DIS studies at the 12 GeV Jefferson Lab [145] could open up a new window on the vector $F_{1,2}^{\gamma Z}$ interference structure functions, as well as provide glimpses into the parity-odd $F_3^{\gamma Z}$ structure function.

For heavier quarks, the issue of intrinsic charm will require measuring the charm structure function at large values of x , which may be possible at a future Electron-Ion Collider facility [113]. The semi-inclusive production of prompt photons and charmed jets in pp collisions at the LHC, $pp \rightarrow \gamma cX$, may produce an enhancement at large transverse momenta from intrinsic charm [267].

Measurements of jet, dijet, isolated γ , and $\gamma + \text{jet}$ production at the LHC will all play a role in helping to further constrain the gluon PDF. Of particular interest would be $\gamma + \text{jet}$ production where both the γ and the jet have equal and opposite large rapidities. The dominant $qg \rightarrow \gamma q$ subprocess would thus require both a high- x gluon and a high- x quark. Furthermore, continued progress on resummation, especially for the fragmentation contribution at fixed target energies may provide additional information on the gluon at high values of x .

In the polarized sector, several experiments planned at Jefferson Lab will measure the longitudinal polarization asymmetries for hydrogen, deuterium and ^3He to unprecedented large values of x [110, 111, 112]. These will constrain the spin-dependent valence quark PDFs, especially the Δd distribution, to values of $x \sim 0.8$. This should help answer long-standing questions about the behavior of the $\Delta q/q$ ratios as $x \rightarrow 1$, and reveal insights into the role of quark orbital angular momentum in the nucleon.

The flavor asymmetry of the polarized light quark sea, $\Delta\bar{u} - \Delta\bar{d}$, will be further probed via W boson production in polarized pp scattering at RHIC at $\sqrt{s} = 510$ GeV. Both the STAR and PHENIX experiments anticipate significantly improved statistics and kinematic coverage in their 2012 and 2013 runs [258]. The strange quark polarization, despite appearing to be smaller than initially surmised from early polarized DIS experiments, is nevertheless important to pin down, as it allows a portal to nonperturbative QCD effects in the nucleon. Improved constraints on kaon fragmentation functions should lead to more reliable determinations of Δs in semi-inclusive DIS.

Finally, the polarized gluon distribution is being actively investigated in semi-inclusive deep-inelastic hadron production at COMPASS, and through double-spin asymmetries for pion and jet production in polarized pp collisions at RHIC. Preliminary results from STAR on jet and dijet cross sections hint at nonzero values for Δg , which

will need to be confirmed by further measurements at small x . Access to Δg below $x \sim 0.05$ will be possible with future running at $\sqrt{s} = 500$ GeV and at large forward rapidity [258], although reaching values down to $x \sim 10^{-4}$ will only be possible with an Electron-Ion Collider [113].

On the theory front, continued progress on NNLO calculations will eventually result in global fits where all the processes are treated consistently at NNLO, for both unpolarized and polarized observables. The increased precision and decreased scale dependence will help to reduce the uncertainty bands on the PDFs. The parametrization dependence of global fits will continue to be explored, allowing for greater flexibility and reducing bias introduced with the use of specific forms, such as for the d/u ratio at large x . Improvements in electroweak radiative corrections are being sought, incorporating, for example, PDFs of a photon with $\mathcal{O}(\alpha) Q^2$ evolution. Progress on computing moments of PDFs in lattice QCD is also anticipated, with more reliable simulations performed on larger lattice volumes and at quark masses near the physical limit. A new approach [268] to calculating the x dependence of the PDFs directly in the infinite momentum frame may provide complementary constraints on PDFs that are difficult to access experimentally.

Acknowledgments

We thank A. Accardi and K. Griffioen for helpful comments and a careful reading of the manuscript. The work of P.J.-D. and W.M. was supported by DOE contract No. DE-AC05-06OR23177, under which Jefferson Science Associates, LLC operates Jefferson Lab. The work of J.F.O. was supported by DOE contract No. DE-FG02-13ER41942.

References

- [1] S. Forte and G. Watt, *Ann. Rev. of Nucl. Part. Sci.* **63**, (2013), arXiv:1301.6754 [hep-ph].
- [2] J. Blümlein, *Prog. Part. Nucl. Phys.* **69**, 28 (2013).
- [3] A. Accardi, *Large- x connections of nuclear and high-energy physics*, to appear in *Mod. Phys. Lett. A*; PoS (Confinement X) 227,
<http://pos.sissa.it/archive/conferences/171/227/Confinement%20X.227.pdf>.
- [4] A. J. Buras, *Rev. Mod. Phys.* **52**, 199 (1980).
- [5] J. F. Owens and W.-K. Tung, *Ann. Rev. Nucl. Part. Sci.* **42**, 291 (1992).
- [6] B. Lampe and E. Reya, *Phys. Rep.* **332**, 1 (2000).
- [7] D. de Florian, R. Sassot, M. Stratmann and W. Vogelsang, *Prog. Part. Nucl. Phys.* **67**, 251 (2012).
- [8] C. A. Aidala, S. D. Bass, D. Hasch and G. K. Mallot, *Rev. Mod. Phys.* **85**, 655 (2013).
- [9] J. Beringer *et al.* [Particle Data Group], *Phys. Rev. D* **86**, 010001 (2012).
- [10] F. J. Yndurain, *The Theory of Quark and Gluon Interactions*, Springer-Verlag (1983).
- [11] V. D. Barger and R. J. N. Phillips, *Collider Physics*, Westview Press (1991).
- [12] R. K. Ellis, W. J. Stirling and B. R. Webber, *QCD and Collider Physics*, Cambridge University Press (1996).
- [13] S. D. Drell and T. M. Yan, *Ann. Phys.* **66**, 578 (1971).
- [14] E. Reya, *Phys. Rep.* **69**, 195 (1981).
- [15] H. Abramowicz *et al.* [H1 and ZEUS Collaborations], *Eur. Phys. J. C* **73**, 2311 (2013).
- [16] M. Glück and E. Reya, *Mod. Phys. Lett. A* **22**, 351 (2007).

- [17] E. Witten, Nucl. Phys. **B104**, 445 (1976).
- [18] J. Babcock, D. W. Sivers and S. Wolfram, Phys. Rev. D **18**, 162 (1978).
- [19] J. P. Leveille and T. J. Weiler, Nucl. Phys. **B147**, 147 (1979).
- [20] M. Glück, E. Hoffmann and E. Reya, Z. Phys. C **13**, 119 (1982).
- [21] E. Laenen, S. Riemersma, J. Smith and W. L. van Neerven, Nucl. Phys. **B392**, 162 (1993).
- [22] S. Riemersma, J. Smith and W. L. van Neerven, Phys. Lett. B **347**, 143 (1995).
- [23] E. Laenen and S.-O. Moch, Phys. Rev. D **59**, 034027 (1999).
- [24] H. Kawamura, N. A. Lo Presti, S.-O. Moch and A. Vogt, Nucl. Phys. **B864**, 399 (2012).
- [25] I. Bierenbaum, J. Blümlein and S. Klein, Nucl. Phys. **B820**, 417 (2009).
- [26] I. Bierenbaum, J. Blümlein and S. Klein, Phys. Lett. B **672**, 401 (2009).
- [27] J. Ablinger, J. Blümlein, A. De Freitas, A. Hasselhuhn, S. Klein, C. Schneider and F. Wißbrock, arXiv:1212.5950 [hep-ph].
- [28] S. Alekhin and S. Moch, Phys. Lett. B **699**, 345 (2011).
- [29] M. Buza, Y. Matiounine, J. Smith and W. L. van Neerven, Eur. Phys. J. C **1**, 301 (1998).
- [30] M. Glück, P. Jimenez-Delgado, E. Reya and C. Schuck, Phys. Lett. B **664**, 133 (2008).
- [31] M. A. G. Aivazis, J. C. Collins, F. I. Olness and W.-K. Tung, Phys. Rev. D **50**, 3102 (1994).
- [32] R. S. Thorne and R. G. Roberts, Phys. Rev. D **57**, 6871 (1998).
- [33] F. M. Steffens, W. Melnitchouk and A. W. Thomas, Eur. Phys. J. C **11**, 673 (1999).
- [34] S. Forte, E. Laenen, P. Nason and J. Rojo, Nucl. Phys. **B834**, 116 (2010).
- [35] J. C. Collins, Phys. Rev. D **58**, 094002 (1998).
- [36] M. Glück, E. Reya and M. Stratmann, Nucl. Phys. **B422**, 37 (1994).
- [37] M. Glück, E. Reya and A. Vogt, Z. Phys. C **67**, 433 (1995).
- [38] M. Glück, E. Reya and A. Vogt, Eur. Phys. J. C **5**, 461 (1998).
- [39] S. Kretzer, H. L. Lai, F. I. Olness and W.-K. Tung, Phys. Rev. D **69**, 114005 (2004).
- [40] S. Alekhin, J. Blümlein and S.-O. Moch, Phys. Rev. D **86**, 054009 (2012).
- [41] M. Glück, P. Jimenez-Delgado and E. Reya, Eur. Phys. J. C **53**, 355 (2008).
- [42] P. Jimenez-Delgado and E. Reya, Phys. Rev. D **80**, 114011 (2009).
- [43] A. D. Martin, W. J. Stirling, R. S. Thorne and G. Watt, Eur. Phys. J. C **63**, 189 (2009).
- [44] H.-L. Lai, M. Guzzi, J. Huston, Z. Li, P. M. Nadolsky, J. Pumplin and C.-P. Yuan, Phys. Rev. D **82**, 074024 (2010).
- [45] J. Gao, M. Guzzi, J. Huston, H. -L. Lai, Z. Li, P. Nadolsky, J. Pumplin, D. Stump and C.-P. Yuan, arXiv:1302.6246 [hep-ph].
- [46] F. D. Aaron *et al.* [H1 and ZEUS Collaborations], JHEP **1001**, 109 (2010).
- [47] R. D. Ball, L. Del Debbio, S. Forte, A. Guffanti, J. I. Latorre, J. Rojo and M. Ubiali, Nucl. Phys. **B838**, 136 (2010).
- [48] W. Melnitchouk, R. Ent and C. Keppel, Phys. Rep. **406**, 127 (2005).
- [49] R. D. Ball *et al.*, Nucl. Phys. **B867**, 244 (2013).
- [50] S. Alekhin, J. Blümlein, S. Klein and S.-O. Moch, Phys. Rev. D **81**, 014032 (2010).
- [51] A. Accardi, M. E. Christy, C. E. Keppel, P. Monaghan, W. Melnitchouk, J. G. Morfin and J. F. Owens, Phys. Rev. D **81**, 034016 (2010).
- [52] A. Accardi, W. Melnitchouk, J. F. Owens, M. E. Christy, C. E. Keppel, L. Zhu and J. G. Morfin, Phys. Rev. D **84**, 014008 (2011).
- [53] J. F. Owens, A. Accardi and W. Melnitchouk, Phys. Rev. D **87**, 094012 (2013).
- [54] H. Georgi and H. D. Politzer, Phys. Rev. D **14**, 1829 (1976).
- [55] S. Matsuda and T. Uematsu, Nucl. Phys. **B168**, 181 (1980).
- [56] A. Piccione and G. Ridolfi, Nucl. Phys. **B513**, 301 (1998).
- [57] J. Blümlein and A. Tkabladze, Nucl. Phys. **B553**, 427 (1999).
- [58] S. Kretzer and M. H. Reno, Phys. Rev. D **69**, 034002 (2004).
- [59] F. M. Steffens, M. D. Brown, W. Melnitchouk and S. Sanches, Phys. Rev. C **86**, 065208 (2012).
- [60] R. K. Ellis, W. Furmanski and R. Petronzio, Nucl. Phys. **B212**, 29 (1983).
- [61] A. Accardi and J.-W. Qiu, JHEP **0807**, 090 (2008).

- [62] A. Accardi, T. J. Hobbs and W. Melnitchouk, JHEP **0911**, 084 (2009).
- [63] A. Accardi, F. Arleo, W. K. Brooks, D. D'Enterria and V. Muccifora, Riv. Nuovo Cim. **32**, 439 (2010).
- [64] I. Schienbein *et al.*, J. Phys. G **35**, 053101 (2008).
- [65] L. T. Brady, A. Accardi, T. J. Hobbs and W. Melnitchouk, Phys. Rev. D **84**, 074008 (2011) [Erratum-*ibid.* D **85**, 039902 (2012)].
- [66] K. Bitar, P. W. Johnson and W.-K. Tung, Phys. Lett. B **83**, 114 (1979); P. W. Johnson and W.-K. Tung, Print-79-1018 (Illinois Tech), *Contribution to Neutrino '79, Bergen, Norway* (1979).
- [67] F. M. Steffens and W. Melnitchouk, Phys. Rev. C **73**, 055202 (2006).
- [68] A. De Rújula, H. Georgi and H. D. Politzer, Phys. Rev. D **15**, 2495 (1977).
- [69] A. De Rújula, H. Georgi and H. D. Politzer, Ann. Phys. **103**, 315 (1977).
- [70] M. Virchaux and A. Milsztajn, Phys. Lett. B **274**, 221 (1992).
- [71] S. I. Alekhin, S. A. Kulagin and S. Liuti, Phys. Rev. D **69**, 114009 (2004).
- [72] J. Blümlein and H. Böttcher, Phys. Lett. B **662**, 336 (2008).
- [73] P. Jimenez-Delgado and E. Reya, in preparation.
- [74] S. Alekhin, S. A. Kulagin and R. Petti, Proceedings of the 15th International Workshop on Deep-Inelastic Scattering and Related Subjects (DIS2007), 16-20 April, 2007, Munich, Germany.
- [75] E. Leader, A. V. Sidorov and D. B. Stamenov, Phys. Rev. D **82**, 114018 (2010).
- [76] J. Blümlein and H. Böttcher, Nucl. Phys. **B841**, 205 (2010).
- [77] J. Blümlein and H. Böttcher, arXiv:1207.3170 [hep-ph].
- [78] A. Accardi, A. Bacchetta, W. Melnitchouk and M. Schlegel, JHEP **0911**, 093 (2009).
- [79] P. Jimenez-Delgado *et al.* [JAM Collaboration], in preparation (2013).
- [80] X. -D. Ji and P. Unrau, Phys. Lett. B **333**, 228 (1994).
- [81] E. Stein, P. Gornicki, L. Mankiewicz and A. Schafer, Phys. Lett. B **353**, 107 (1995).
- [82] Z. E. Meziani *et al.*, Phys. Lett. B **613**, 148 (2005).
- [83] A. Deur *et al.*, Phys. Rev. Lett. **93**, 212001 (2004).
- [84] M. Osipenko *et al.*, Phys. Lett. B **609**, 259 (2005).
- [85] J. J. Aubert *et al.* [European Muon Collaboration], Phys. Lett. B **123**, 123 (1983).
- [86] D. F. Geesaman, K. Saito and A. W. Thomas, Ann. Rev. Nucl. Part. Sci. **45**, 337 (1995).
- [87] P. R. Norton, Rept. Prog. Phys. **66**, 1253 (2003).
- [88] W. Melnitchouk, A. W. Schreiber and A. W. Thomas, Phys. Rev. D **49**, 1183 (1994).
- [89] S. A. Kulagin, G. Piller and W. Weise, Phys. Rev. C **50**, 1154 (1994).
- [90] S. A. Kulagin and R. Petti, Nucl. Phys. **A765**, 126 (2006).
- [91] Y. Kahn, W. Melnitchouk and S. A. Kulagin, Phys. Rev. C **79**, 035205 (2009).
- [92] A. D. Martin, A. J. T. M. Mathijssen, W. J. Stirling, R. S. Thorne, B. J. A. Watt and G. Watt, Eur. Phys. J. C **73**, 2318 (2013).
- [93] R. B. Wiringa, V. G. J. Stoks and R. Schiavilla, Phys. Rev. C **51**, 38 (1995).
- [94] R. Machleidt, Phys. Rev. C **63**, 024001 (2001).
- [95] F. Gross and A. Stadler, Phys. Rev. C **78**, 014005 (2008); *ibid.* C **82**, 034004 (2010).
- [96] R. D. Ball *et al.*, Phys. Lett. B **723**, 330 (2013).
- [97] J. Arrington, F. Coester, R. J. Holt and T.-S. H. Lee, J. Phys. G **36**, 025005 (2009).
- [98] J. Arrington, J. G. Rubin and W. Melnitchouk, Phys. Rev. Lett. **108**, 252001 (2012).
- [99] S. Kuhlmann *et al.*, Phys. Lett. B **476**, 291 (2000).
- [100] L. T. Brady, A. Accardi, W. Melnitchouk and J. F. Owens, JHEP **1206**, 019 (2012).
- [101] A. O. Bazarko *et al.* [CCFR Collaboration], Z. Phys. C **65**, 189 (1995).
- [102] D. Mason *et al.* [NuTeV Collaboration], Phys. Rev. Lett. **99**, 192001 (2007).
- [103] S. A. Kulagin and R. Petti, Phys. Rev. D **76**, 094023 (2007).
- [104] I. Schienbein, J. Y. Yu, K. Kovarik, C. Keppel, J. G. Morfin, F. Olness and J. F. Owens, Phys. Rev. D **80**, 094004 (2009).
- [105] M. Hirai, S. Kumano and T. -H. Nagai, Phys. Rev. C **76**, 065207 (2007).

- [106] K. J. Eskola, H. Paukkunen and C. A. Salgado, JHEP **0904**, 065 (2009).
- [107] K. Kovarik, I. Schienbein, F. I. Olness, J. Y. Yu, C. Keppel, J. G. Morfin, J. F. Owens and T. Stavreva, Phys. Rev. Lett. **106**, 122301 (2011).
- [108] H. Paukkunen and C. A. Salgado, Phys. Rev. Lett. **110**, 212301 (2013).
- [109] D. de Florian, R. Sassot, P. Zurita and M. Stratmann, Phys. Rev. D **85**, 074028 (2012).
- [110] Jefferson Lab Experiment E12-06-109, *The Longitudinal Spin Structure of the Nucleon*, D. Crabb *et al.*, spokespersons.
- [111] Jefferson Lab Experiment E12-06-110, *Measurement of the Neutron Spin Asymmetry A_1^n in the Valence Quark Region Using an 11 GeV Beam in Hall C*, J.-P. Chen *et al.*, spokespersons.
- [112] Jefferson Lab Experiment E12-06-122, *Measurement of the Neutron Asymmetry A_1^n in the Valence Quark Region Using 8.8 and 6.6 GeV Beam Energies and the BigBite Spectrometer in Hall A*, B. Wojtsekhowski *et al.*, spokespersons.
- [113] A. Accardi *et al.*, *Electron Ion Collider: The Next QCD Frontier - Understanding the glue that binds us all*, BNL-98815-2012-JA, JLAB-PHY-12-1652, arXiv:1212.1701 [nucl-ex].
- [114] C. Bourrely, J. Soffer and F. Buccella, Eur. Phys. J. C **23**, 487 (2002).
- [115] S. Forte, L. Garrido, J. I. Latorre and A. Piccione, JHEP **0205**, 062 (2002).
- [116] H. Honkanen, S. Liuti, J. Carnahan, Y. Loitiere and P. R. Reynolds, Phys. Rev. D **79**, 034022 (2009).
- [117] F. E. Close and R. G. Roberts, Phys. Lett. B **316**, 165 (1993).
- [118] J. Pumplin *et al.*, Phys. Rev. D **65**, 014013 (2001).
- [119] D. Stump *et al.*, Phys. Rev. D **65**, 014012 (2001).
- [120] L. D. Debbio *et al.*, JHEP **0703**, 039 (2007).
- [121] D. Stump *et al.*, JHEP **0310**, 046 (2003).
- [122] P. Jimenez-Delgado, Phys. Lett. B **714**, 301 (2012).
- [123] J. Pumplin *et al.*, JHEP **0207**, 012 (2003).
- [124] T. Aaltonen *et al.* [CDF Collaboration], Phys. Rev. Lett. **102**, 181801 (2009).
- [125] G. Aad *et al.* [ATLAS Collaboration], Phys. Rev. Lett. **109**, 012001 (2012).
- [126] D. de Florian and W. Vogelsang, Phys. Rev. D **72**, 014014 (2005).
- [127] P. Aurenche *et al.*, Eur. Phys. J. **C9**, 107 (1999).
- [128] P. Aurenche *et al.*, Phys. Rev. D **73**, 094007 (2006).
- [129] D. d'Enterria and J. Rojo, Nucl. Phys. **B860**, 311 (2012).
- [130] E. L. Berger and J. -w. Qiu, Phys. Rev. D **40**, 778 (1989).
- [131] CTEQ Collaboration website, <http://www.cteq.org>.
- [132] R. P. Feynman, *Photon Hadron Interactions* (Benjamin, Reading, Massachusetts, 1972).
- [133] F. E. Close, Phys. Lett. B **43**, 422 (1973).
- [134] W. Melnitchouk and A. W. Thomas, Phys. Lett. B **377**, 11 (1996).
- [135] R. J. Holt and C. D. Roberts, Rev. Mod. Phys. **82**, 2991 (2010).
- [136] G. R. Farrar and D. R. Jackson, Phys. Rev. Lett. **35**, 1416 (1975).
- [137] R. Blankenbecler and S. J. Brodsky, Phys. Rev. D **10**, 2973 (1974).
- [138] J. F. Gunion, Phys. Rev. D **10**, 242 (1974).
- [139] S. J. Brodsky and G. P. Lepage, Proceedings of the 1979 Summer Institute on Particle Physics, SLAC (1979).
- [140] Y. Itow *et al.* [T2K Collaboration], KEK-REPORT-2001-4, arXiv:hep-ex/0106019.
- [141] D. S. Ayres *et al.* [NOvA Collaboration], FERMILAB-PROPOSAL-0929, arXiv:hep-ex/0503053.
- [142] S. Raby *et al.*, SLAC-PUB-14734, arXiv:0810.4551 [hep-ph].
- [143] Jefferson Lab Experiment E12-10-102 [BONUS12], *The Structure of the Free Neutron at Large x -Bjorken*, S. Bültmann, M. E. Christy, H. Fenker, K. Griffioen, C. E. Keppel, S. Kuhn and W. Melnitchouk, spokespersons.
- [144] Jefferson Lab Experiment E12-10-103 [MARATHON], *Measurement of the F_2^n/F_2^p , d/u Ratios and $A = 3$ EMC Effect in DIS off the Tritium and Helium Mirror Nuclei*, G. G. Petratos, J. Gomez, R. J. Holt and R. D. Ransome, spokespersons.

- [145] Jefferson Lab Experiment E12-10-007 [SoLID], P. Souder, spokesperson.
- [146] J. L. Abelleira Fernandez *et al.* [LHeC Study Group], *On the Relation of the LHeC and the LHC*, arXiv:1211.5102 [hep-ex].
- [147] CTEQ-Jefferson Lab (CJ) Collaboration website, <http://www.jlab.org/cj>.
- [148] S. D. Drell and T. -M. Yan, Phys. Rev. Lett. **25**, 316 (1970) [Erratum-ibid. **25**, 902 (1970)].
- [149] A. Baldit *et al.* [NA51 Collaboration], Phys. Lett. B **332**, 244 (1994).
- [150] E. A. Hawker *et al.* [FNAL E866/NuSea Collaboration], Phys. Rev. Lett. **80**, 3715 (1998).
- [151] R. S. Towell *et al.* [FNAL E866/NuSea Collaboration], Phys. Rev. D **64**, 052002 (2001).
- [152] D. A. Ross and C. T. Sachrajda, Nucl. Phys. **B149**, 497 (1979).
- [153] P. Amaudruz *et al.* [New Muon Collaboration], Phys. Rev. Lett. **66**, 2712 (1991).
- [154] M. Arneodo *et al.* [New Muon Collaboration], Phys. Rev. D **50**, 1 (1994).
- [155] K. Gottfried, Phys. Rev. Lett. **18**, 1174 (1967).
- [156] S. D. Ellis and W. J. Stirling, Phys. Lett. B **256**, 258 (1991).
- [157] R. D. Field and R. P. Feynman, Phys. Rev. D **15**, 2590 (1977).
- [158] A. W. Schreiber, A. I. Signal and A. W. Thomas, Phys. Rev. D **44**, 2653 (1991).
- [159] A. I. Signal, A. W. Schreiber and A. W. Thomas, Mod. Phys. Lett. A **6**, 271 (1991).
- [160] F. M. Steffens and A. W. Thomas, Phys. Rev. C **55**, 900 (1997).
- [161] A. W. Thomas, Phys. Lett. B **126**, 97 (1983).
- [162] J. Speth and A. W. Thomas, Adv. Nucl. Phys. **24**, 83 (1997).
- [163] S. Kumano, Phys. Rep. **303**, 183 (1998).
- [164] A. W. Thomas, W. Melnitchouk and F. M. Steffens, Phys. Rev. Lett. **85**, 2892 (2000).
- [165] M. Burkardt, K. S. Hendricks, C. -R. Ji, W. Melnitchouk and A. W. Thomas, Phys. Rev. D **87**, 056009 (2013).
- [166] Fermilab E906 experiment, *Drell-Yan Measurements of Nucleon and Nuclear Structure with the Fermilab Main Injector*, D. F. Geesaman and P. E. Reimer, spokespersons; <http://www.phy.anl.gov/mep/SeaQuest/index.html>.
- [167] J-PARC proposal P04, *Measurement of High-Mass Dimuon Production at the 50-GeV Proton Synchrotron*, J. C. Peng and S. Sawada spokespersons; <http://j-parc.jp/index-e.html>.
- [168] S. Kumano, J. Phys. Conf. Ser. **312**, 032005 (2011).
- [169] E. Sather, Phys. Lett. B **274**, 433 (1992).
- [170] E. N. Rodionov, A. W. Thomas and J. T. Londergan, Mod. Phys. Lett. A **9**, 1799 (1994).
- [171] J. T. Londergan and A. W. Thomas, Phys. Lett. B **558**, 132 (2003).
- [172] J. T. Londergan, J. C. Peng and A. W. Thomas, Rev. Mod. Phys. **82**, 2009 (2010).
- [173] M. Gluck, P. Jimenez-Delgado and E. Reya, Phys. Rev. Lett. **95**, 022002 (2005).
- [174] A. D. Martin, R. G. Roberts, W. J. Stirling and R. S. Thorne, Eur. Phys. J. C **39**, 155 (2005).
- [175] G. P. Zeller *et al.* [NuTeV Collaboration], Phys. Rev. Lett. **88**, 091802 (2002) [Erratum-ibid. **90**, 239902 (2003)].
- [176] E. A. Paschos and L. Wolfenstein, Phys. Rev. D **7**, 91 (1973).
- [177] P. Jimenez-Delgado, Phys. Lett. B **689**, 177 (2010).
- [178] A. I. Signal and A. W. Thomas, Phys. Lett. B **191**, 205 (1987).
- [179] M. Burkardt and B. Warr, Phys. Rev. D **45**, 958 (1992).
- [180] W. Melnitchouk and M. Malheiro, Phys. Rev. C **55**, 431 (1997).
- [181] J. Alwall and G. Ingelman, Phys. Rev. D **70**, 111505 (2004).
- [182] S. Catani, D. de Florian, G. Rodrigo and W. Vogelsang, Phys. Rev. Lett. **93**, 152003 (2004).
- [183] T. Gottschalk, Phys. Rev. D **23**, 56 (1981).
- [184] M. Glück, S. Kretzer and E. Reya, Phys. Lett. B **380**, 171 (1996) [Erratum-ibid. B **405**, 391 (1997)].
- [185] S. Kretzer, D. Mason and F. Olness, Phys. Rev. D **65**, 074010 (2002).
- [186] F. Olness *et al.*, Eur. Phys. J. C **40**, 145 (2005).
- [187] D. de Florian and R. Sassot, Phys. Rev. D **69**, 074028 (2004).
- [188] B. W. Harris and J. Smith, Phys. Rev. D **57**, 2806 (1998).

- [189] S. J. Brodsky, P. Hoyer, C. Peterson and N. Sakai, Phys. Lett. B **93**, 451 (1980).
- [190] R. Vogt, Nucl. Phys. **B446**, 159 (1995).
- [191] F. S. Navarra, M. Nielsen, C. A. A. Nunes and M. Teixeira, Phys. Rev. D **54**, 842 (1996).
- [192] R. Vogt, Prog. Part. Nucl. Phys. **45**, S105 (2000).
- [193] J. Pumplin, Phys. Rev. D **73**, 114015 (2006).
- [194] J. J. Aubert *et al.* [European Muon Collaboration], Phys. Lett. B **110**, 73 (1982).
- [195] J. J. Aubert *et al.* [European Muon Collaboration], Nucl. Phys. **B213**, 31 (1983).
- [196] B. W. Harris, J. Smith and R. Vogt, Nucl. Phys. **B461**, 181 (1996).
- [197] T. J. Hobbs, J. T. Londergan and W. Melnitchouk, in preparation.
- [198] Workshop on Future Prospects of Hadron Physics at J-PARC and Large Scale Computational Physics in 2013, <http://j-parc-th.kek.jp/html/English/JPARCFeb2013.html>.
- [199] J. Riedl, A. Schäfer and M. Stratmann, Eur. Phys. J. C **52**, 987 (2007).
- [200] Jefferson Lab proposal PR12-07-106, *The A-dependence of J/ψ photoproduction near threshold*, E. Chudakov *et al.*, spokespersons.
- [201] N. Brambilla *et al.*, Eur. Phys. J. C **71**, 1534 (2011).
- [202] S. J. Brodsky, F. Fleuret, C. Hadjidakis and J. P. Lansberg, Phys. Rep. **522**, 239 (2013).
- [203] P. Monaghan, A. Accardi, M. E. Christy, C. E. Keppel, W. Melnitchouk and L. Zhu, Phys. Rev. Lett. **110**, 152002 (2013).
- [204] E. L. Berger, L. E. Gordon and M. Klasen, Phys. Rev. D **58**, 074012 (1998).
- [205] L. Carminati *et al.*, Europhys. Lett. **101**, 61002 (2013),
- [206] M. Czakon *et al.*, arXiv:1303.7215 [hep-ph].
- [207] M. Mangano and J. Rojo, JHEP **1208**, 010 (2012).
- [208] A. G.-D. Ridder, T. Gehrmann, E. W. N. Glover and J. Pires, Phys. Rev. Lett. **110**, 162003 (2013).
- [209] P. Jimenez-Delgado and E. Reya, Phys. Rev. D **79**, 074023 (2009).
- [210] W. Detmold, W. Melnitchouk and A. W. Thomas, Eur. Phys. J. direct C **3**, 1 (2001).
- [211] J. D. Bratt *et al.* [LHP Collaboration], Phys. Rev. D **82**, 094502 (2010).
- [212] D. Pleiter *et al.* [QCDSF/UKQCD Collaboration], PoS LATTICE **2010**, 153 (2010).
- [213] W. Detmold, W. Melnitchouk, J. W. Negele, D. B. Renner and A. W. Thomas, Phys. Rev. Lett. **87**, 172001 (2001).
- [214] M. Procura, B. U. Musch, T. R. Hemmert and W. Weise, Phys. Rev. D **75**, 014503 (2007).
- [215] P. E. Shanahan, A. W. Thomas and R. D. Young, arXiv:1301.6861 [nucl-th].
- [216] W. Detmold, W. Melnitchouk and A. W. Thomas, Phys. Rev. D **66**, 054501 (2002).
- [217] J. Ashman *et al.* [European Muon Collaboration], Phys. Lett. B **206**, 364 (1988); Nucl. Phys. **B328**, 1 (1989).
- [218] B. Adeva *et al.* [Spin Muon Collaboration], Phys. Rev. D **58**, 112001 (1998); Phys. Rev. D **60**, 072004 (1999) [Erratum-ibid. D **62**, 079902 (2000)].
- [219] V. Yu. Alexakhin *et al.* [COMPASS Collaboration], Phys. Lett. B **647**, 8 (2007).
- [220] M. G. Alekseev *et al.* [COMPASS Collaboration], Phys. Lett. B **690**, 466 (2010).
- [221] B. Adeva *et al.* [Spin Muon Collaboration], Phys. Lett. B **420**, 180 (1998).
- [222] M. G. Alekseev *et al.* [COMPASS Collaboration], Phys. Lett. B **693**, 227 (2010).
- [223] G. Baum *et al.*, Phys. Rev. Lett. **51**, 1135 (1983).
- [224] P. L. Anthony *et al.* [SLAC E142 Collaboration], Phys. Rev. D **54**, 6620 (1996).
- [225] K. Abe *et al.* [SLAC E154 Collaboration], Phys. Rev. Lett. **79**, 26 (1997).
- [226] K. Abe *et al.* [SLAC E143 Collaboration], Phys. Rev. D **58**, 112003 (1998).
- [227] P. L. Anthony *et al.* [SLAC E155 Collaboration], Phys. Lett. B **458**, 529 (1999); Phys. Lett. B **463**, 339 (1999); Phys. Lett. B **493**, 19 (2000).
- [228] P. L. Anthony *et al.* [SLAC E155x Collaboration], Phys. Lett. B **553**, 18 (2003).
- [229] K. Ackerstaff *et al.* [HERMES Collaboration], Phys. Lett. B **404**, 383 (1997).
- [230] A. Airapetian *et al.* [HERMES Collaboration], Phys. Rev. D **75**, 012007 (2007).
- [231] A. Airapetian *et al.* [HERMES Collaboration], Eur. Phys. J. C **72**, 1921 (2012).

- [232] A. Airapetian *et al.* [HERMES Collaboration], Phys. Rev. D **71**, 012003 (2005).
- [233] A. Airapetian *et al.* [HERMES Collaboration], Phys. Lett. B **666**, 446 (2008).
- [234] X. Zhang *et al.* [Jefferson Lab E99-117 Collaboration], Phys. Rev. Lett. **92**, 012004 (2004); Phys. Rev. C **70**, 065207 (2004).
- [235] K. Kramer *et al.* [Jefferson Lab E97-103 Collaboration], Phys. Rev. Lett. **95**, 142002 (2005).
- [236] P. Solvignon *et al.* [Jefferson Lab E01-012 Collaboration], Phys. Rev. Lett. **101**, 182502 (2008); arXiv:1304.4497 [nucl-ex].
- [237] K. V. Dharmawardane *et al.* [CLAS Collaboration], Phys. Lett. B **641**, 11 (2006).
- [238] Y. Prok *et al.* [CLAS Collaboration], Phys. Lett. B **672**, 12 (2009).
- [239] D. L. Adams *et al.* [FNAL E581/704 Collaboration], Phys. Lett. B **336**, 269 (1994).
- [240] A. Adare *et al.* [PHENIX Collaboration], Phys. Rev. Lett. **103**, 012003 (2009).
- [241] A. Manion [PHENIX Collaboration], J. Phys. Conf. Ser. **295**, 012070 (2011).
- [242] M. M. Aggarwal *et al.* [STAR Collaboration], Phys. Rev. Lett. **106**, 062002 (2011).
- [243] L. Adamczyk *et al.* [STAR Collaboration], Phys. Rev. D **86**, 032006 (2012).
- [244] P. Djawotho [STAR Collaboration], XIX International Workshop on Deep-Inelastic Scattering and Related Subjects (DIS 2011), arXiv:1106.5769 [nucl-ex].
- [245] D. de Florian, R. Sassot, M. Stratmann and W. Vogelsang, Phys. Rev. D **80**, 034030 (2009).
- [246] M. Hirai and S. Kumano, Nucl. Phys. **B813**, 106 (2009).
- [247] R. D. Ball *et al.*, arXiv:1303.7236 [hep-ph].
- [248] C. Adolph *et al.* [COMPASS Collaboration], Phys. Rev. D **87**, 052018 (2013).
- [249] J. Arrington, C. D. Roberts and J. M. Zanotti, J. Phys. G **34**, S23 (2007).
- [250] W. Melnitchouk, Phys. Rev. Lett. **86**, 35 (2001) [Erratum-ibid. **93**, 199901 (2004)].
- [251] E. D. Bloom and F. J. Gilman, Phys. Rev. Lett. **25**, 1140 (1970).
- [252] H. Avakian, S. J. Brodsky, A. Deur and F. Yuan, Phys. Rev. Lett. **99**, 082001 (2007)
- [253] Jefferson Lab Experiment E12-06-121, *A Path to Color Polarizabilities*, Z.-E. Meziani *et al.*, spokespersons.
- [254] M. Wakamatsu, Phys. Rev. D **44**, 2631 (1991).
- [255] P. V. Pobylitsa, M. V. Polyakov, K. Goeke, T. Watabe and C. Weiss, Phys. Rev. D **59**, 034024 (1999).
- [256] C. Bourrely and J. Soffer, Phys. Lett. B **314**, 132 (1993).
- [257] D. de Florian and W. Vogelsang, Phys. Rev. D **81**, 094020 (2010).
- [258] E. C. Aschenauer *et al.*, arXiv:1304.0079 [nucl-ex].
- [259] M. Walker [STAR Collaboration], XIX International Workshop on Deep-Inelastic Scattering and Related Subjects (DIS 2011), arXiv:1107.0917 [hep-ex].
- [260] A. Airapetian *et al.* [HERMES Collaboration], in print; H. Jackson, talk given at the *XXI International Workshop on Deep-Inelastic Scattering and Related Subjects (DIS2013)*, Marseilles, France, April 22-26, 2013.
- [261] Jefferson Lab Experiment E12-09-002, *Precise Measurement of π^+/π^- Ratios Semi-Inclusive DIS: Charge Symmetry Violating Quark Distributions*, K. Hafidi *et al.*, spokespersons.
- [262] C. Y. Prescott *et al.*, Phys. Lett. B **77**, 347 (1978).
- [263] D. Wang *et al.* [Jefferson Lab Hall A Collaboration], arXiv:1304.7741 [nucl-ex].
- [264] J. D. Bjorken, Phys. Rev. D **18**, 3239 (1978).
- [265] T. Hobbs and W. Melnitchouk, Phys. Rev. D **77**, 114023 (2008).
- [266] S. Mantry, M. J. Ramsey-Musolf and G. F. Sacco, Phys. Rev. C **82**, 065205 (2010).
- [267] V. A. Bednyakov, M. A. Demichev, G. I. Lykasov, T. Stavreva and M. Stockton, arXiv:1305.3548 [hep-ph].
- [268] X. Ji, Phys. Rev. Lett. **110**, 262002 (2013).